Pergamon

J. Mech. Phys. Solids, Vol. 43, No. 12, pp. 1887–1918, 1995

0022–5096/95 $9.50+0.00

0022–5096(95)00057–7

MICROBUCKLE INITIATION IN FIBRE COMPOSITES: A FINITE ELEMENT STUDY

NORMAN A. FLECK and JOHN Y. SHU

Cambridge University Engineering Department, Trumpington Street, Cambridge CB2 1PZ, U.K.

(*Received* 20 *February* 1995; *in revised form* 29 *June* 1995)

ABSTRACT

A finite strain continuum theory is presented for unidirectional fibre reinforced composites under in-plane loading. The constitutive response is expressed in terms of couple stress theory, and is deduced from a unit cell of a linear elastic Timoshenko beam embedded in a non-linear elastic–plastic matrix. The continuum theory is implemented within a finite element framework and is used to analyse compressive failure of polymer matrix composites by fibre microbuckling. It is assumed that microbuckling initiates from an imperfection in the form of a finite elliptical region of fibre waviness. The calculations show that the compressive strength decreases with increasing imperfection spatial size from the elastic bifurcation value of Rosen (1965, *Fibre Composite Materials*, pp. 37–75, American Society Metals Seminar) to the imperfection-sensitive infinite band strength given by Fleck *et al.* [1995, *J. Appl. Mech.* **62,** 329–337.].

1. INTRODUCTION

Compressive failure is a design limiting feature of long fibre–polymer matrix composites since their compressive strength is about 60% of their tensile strength. Rosen (1965) predicted the compressive strength of fibre composites by assuming that microbuckling is an elastic bifurcation; these calculations over-estimate the strength by a factor of about four. Subsequently, Argon (1972) and Budiansky and Fleck (1993) have shown that microbuckling is governed by the plastic deformation of the matrix and by the degree of initial fibre misalignment: the composite fails by imperfection-sensitive plastic buckling.

To date most analyses of localisation in solids, including plastic microbuckling, are one-dimensional calculations based on the response of an infinite band as outlined by Rice (1976). For example, Hutchinson and Tvergaard (1981) have performed an infinite shear band analysis to estimate the plane strain ductility of metallic alloys; they found that the ductility is sensitive to the magnitude of imperfections (in the form of a lower yield strength within the infinite band) and that elastic and plastic bifurcation calculations grossly overestimate the strain to failure (and the associated strength). Budiansky (1983) and Budiansky and Fleck (1993) came to the same conclusions for plastic microbuckling of fibre composites: imperfections are needed in the analysis in order to predict realistic compressive strengths. There are a number of sources of imperfection, including fibre waviness, and voids and cracks within the matrix.

The infinite band analyses described above suffer from two main limitations:

(i) they are unable to predict the width of the microbuckle band, as the constitutive law contains no length scale; and
(ii) they assume that the initial imperfection exists as an infinite band rather than as a finite region. Fleck *et al.* (1995) overcame the first limitation by performing an infinite band analyses using a constitutive law which involved the fibre diameter as the pertinent length scale. They assumed that the fibres possess a finite bending resistance (which depends upon the fibre diameter) and used couple stress theory to predict the broadening of the microbuckle band from an initial infinite band of fibre misalignment. The final width of the microbuckle band is set by fibre fracture: it was assumed that the fibres break when the maximum tensile bending strain in the fibres equals the tensile failure strain of the fibres. Fleck *et al.* (1995) predict that the final width of the microbuckle band is 10–20 fibre diameters, and that the width is relatively insensitive to both the constitutive properties of the composite, and the initial width and magnitude of fibre misalignment. In contrast, the compressive strength was found to be sensitive to the fibre misalignment angle and moderately sensitive to the width of the initial band of misaligned fibres.

Recently, a related finite element analysis has been performed by Kyriakides *et al.* (1995) to study the early stages of microbuckling. They treated the fibres and matrix as discrete but perfectly-bonded layers. This approach is useful when the initial region of fibre waviness extends over only a small number of fibres, but becomes prohibitively expensive in computer time when a large number of fibres are considered. In the current work we follow the approach of Fleck *et al.* (1995) and "smear-out" the effect of the individual fibres by modelling the composite as a Cosserat continuum capable of bearing couple stresses. In a finite element realisation of the Cosserat couple stress theory, each element represents a domain of the composite which may contain many embedded fibres.

Scope of the paper

In the current work both of the above limitations to an infinite band analysis are addressed: we develop a constitutive law with fibre diameter as length scale, and we examine the initiation and early growth of a microbuckle from an elliptical region of initial fibre waviness. The fibre composite is treated as a smeared-out Cosserat continuum, with a bending resistance set by the fibre diameter d. In order to obtain the constitutive law, the fibres are assumed to behave as elastic Timoshenko beams embedded within a non-linear dilitant plastic matrix. A virtual work expression is obtained for a two-dimensional unit cell consisting of a fibre of volume fraction c adhered to a matrix of volume fraction $(1-c)$. Macroscopic stress and strain quantities are thereby derived for the smeared-out homogeneous composite. It is found that the governing equations are identical to those of Cosserat couple stress theory (Cosserat and Cosserat, 1909). The significance of the unit cell analysis is that the *independent micro rotation angle* θ in the general couple stress theory is shown to be the *independent rotation angle* θ_f of the fibre cross-section. A constitutive law for the composite is proposed wherein the bending resistance of the fibres is set by the fibre diameter d.

The governing field equations and constitutive law for the fibre composite is implemented via a finite element code, using 6-noded triangular elements with three degrees of freedom at each node (two displacements and one rotation). The finite element procedure is based upon a Lagrangian formulation of the general finite deformation of the composite, and can deal with both geometrical and material non-linearities. A version of the modified Riks algorithm (Crisfield, 1991) is adopted to handle snap-back behaviour associated with the microbuckling response. Imperfections in the form of fibre waviness are included in the formulation.

The finite element code is used in the first instance to determine the effect of a finite region of initial waviness upon the compressive strength of the composite. The initial stages of propagation of a finite microbuckle band are also addressed.

2. TWO-DIMENSIONAL COSSERAT THEORY FOR A FIBROUS SOLID

In a classical continuum theory an arbitrary surface element of the material is able to bear force tractions but cannot support torque tractions. For the case of fibre composites it is plausible that the fibres carry a substantial bending moment when the curvature imposed on the material is large. Under these circumstances, a "smeared-out" material element is capable of supporting a local bending moment per unit area, known as a *couple stress*. Fleck *et al.* (1995) conducted a one-dimensional infinite band analysis of microbuckling using couple stress theory. They assumed that the fibre rotation is equal to the material rotation, and so their analysis fits within the framework of *reduced* Cosserat theory. Here, we shall consider a two-dimensional version of *general* Cosserat theory, in which the rotation kinematic quantity is independent of the material rotation.

The governing kinematic, equilibrium and virtual work relations are now derived for the in-plane deformation of a unidirectional fibre composite; the formulation fits within the framework of general Cosserat theory, which is summarised for the full three-dimensional case in Appendix A. A Lagrangian formulation is employed to describe the deformed configuration in terms of the initial reference configuration.

2.1. *Kinematics*

We treat a long fibre–matrix composite as a "smeared-out" homogeneous anisotropic solid with effective properties to be derived in Section 4 below. Cartesian base vectors $(\mathbf{e}_1, \mathbf{e}_2)$ are introduced within the plane of deformation, and are oriented such that the $\mathbf{e}_1$-direction is taken to be parallel to the fibre direction of the fully aligned unidirectional composite in the initial configuration. The unit normal to the plane of deformation is given by the Cartesian base vector $\mathbf{e}_3 = \mathbf{e}_1 \times \mathbf{e}_2$. A material point is identified by the position vector $\mathbf{x}$ in the initial undeformed configuration, and undergoes a finite in-plane displacement $\mathbf{u}$ to a position $\mathbf{X}$ in the current, deformed configuration as shown in Fig. 1. The vectors $\mathbf{x}$, $\mathbf{u}$ and $\mathbf{X}$ may be expressed in terms of their Cartesian co-ordinates x_i, u_i and X_i as

$$\mathbf{x} = x_i \mathbf{e}_i, \quad \mathbf{u} = u_i \mathbf{e}_i \quad \text{and} \quad \mathbf{X} = X_i \mathbf{e}_i \tag{2.1}$$

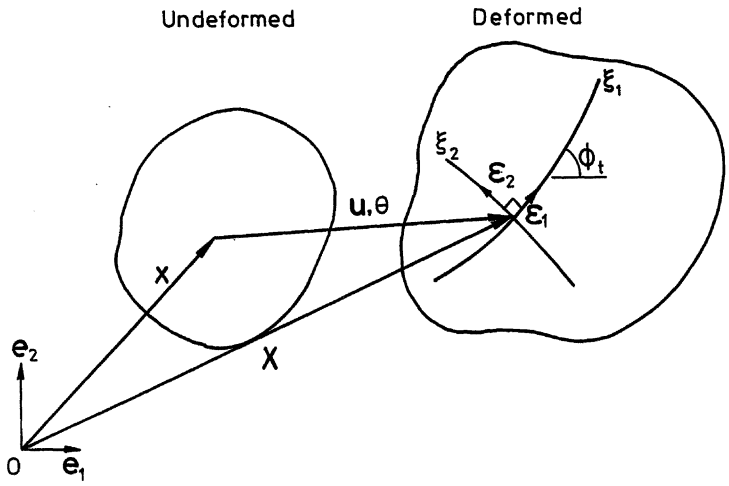

Fig. 1. Definition of co-ordinates and base vectors.

respectively. Here and elsewhere a repeated suffix denotes summation over 1 and 2 unless stated otherwise. We assume that the fibres have an initial misalignment in the form of a rotation $\bar{\phi}(\mathbf{x})$ about the $\mathbf{e}_3$-axis, and upon deformation the fibres rotate through an additional angle $\phi(\mathbf{x})$ about the $\mathbf{e}_3$-axis to a total misalignment of $\phi_t = \bar{\phi} + \phi$. It is convenient to introduce an orthogonal curvilinear co-ordinate system (ξ_1, ξ_2) in the deformed configuration, and to align the ξ_1-direction with the deformed fibre direction (see Fig. 1). The physical distance along the ξ_1-direction is denoted by s_1 and the physical distance along the ξ_2-direction is denoted by s_2. The curvilinear co-ordinate system (ξ_1, ξ_2) is fully specified upon selecting arbitrarily a fibre as the base curve $\xi_2 = 0$ along which $\xi_1 = s_1$, and an orthogonal base curve $\xi_1 = 0$ along which $\xi_2 = s_2$. In our development, tensors such as stress and strain will be expressed in terms of their physical components with respect to the co-ordinate system (ξ_1, ξ_2); spatial gradients in the deformed configuration will also be expressed in terms of s_1 and s_2. With ϕ_t defined as the angle between the ξ_1-axis and the X_1-axis, the unit base vectors $(\boldsymbol{\varepsilon}_1, \boldsymbol{\varepsilon}_2)$ of the curvilinear co-ordinate system are related to the Cartesian base vectors $\mathbf{e}_i$ by

$$\boldsymbol{\varepsilon}_1 = \cos\phi_t \mathbf{e}_1 + \sin\phi_t \mathbf{e}_2 \quad \text{and} \quad \boldsymbol{\varepsilon}_2 = -\sin\phi_t \mathbf{e}_1 + \cos\phi_t \mathbf{e}_2. \tag{2.2}$$

The displacement $\mathbf{u}$ and the velocity $\mathbf{v}$ of a material point may be expressed in terms of the base vectors $\mathbf{e}_i$ and $\boldsymbol{\varepsilon}_i$ as

$$\mathbf{u} = \mathbf{X} - \mathbf{x} = u_i \mathbf{e}_i = U_i \boldsymbol{\varepsilon}_i \tag{2.3a}$$

and

$$\mathbf{v} = \dot{\mathbf{u}} = \dot{\mathbf{X}} = v_i \mathbf{e}_i = V_i \boldsymbol{\varepsilon}_i \tag{2.3b}$$

where the ascent dot denotes the material time derivative. The virtual displacement $\delta\mathbf{u}$ may be expressed in similar manner as

$$\delta\mathbf{u} = \delta\mathbf{X} = \delta u_i \mathbf{e}_i = \delta U_i \boldsymbol{\varepsilon}_i. \tag{2.3c}$$

Note that U_i, V_i and δU_i are defined as the physical components of the displacement,

velocity and virtual displacement, respectively, in terms of the orthonormal base vectors $(\boldsymbol{\varepsilon}_1, \boldsymbol{\varepsilon}_2)$. In two-dimensional Cosserat theory a rotation $\boldsymbol{\theta}$ is introduced as an *independent* kinematic quantity of the form

$$\boldsymbol{\theta} \equiv \theta \mathbf{e}_3. \tag{2.4a}$$

In Section 3 below we shall identify $\boldsymbol{\theta}$ with the rotation of the fibre cross-section. In like manner, the virtual rotation $\delta\boldsymbol{\theta}$ is written as

$$\delta\boldsymbol{\theta} = \delta\theta \mathbf{e}_3. \tag{2.4b}$$

The velocity gradient $\mathbf{D} = \hat{\nabla}\mathbf{v}$ in the deformed configuration can be expressed in the curvilinear co-ordinate system as

$$\mathbf{D} \equiv \hat{\nabla}\mathbf{v} = \boldsymbol{\varepsilon}_i \frac{\partial}{\partial s_i}(V_j \boldsymbol{\varepsilon}_j) = \mathrm{D}_{ij}\boldsymbol{\varepsilon}_i\boldsymbol{\varepsilon}_j. \tag{2.5a}$$

Here, the components D_{ij} are expressed in terms of the physical distances s_i as

$$\left.\begin{aligned} D_{11} &= \frac{\partial V_1}{\partial s_1} - V_2 \frac{\partial \phi_t}{\partial s_1}, \quad D_{12} = \frac{\partial V_2}{\partial s_1} + V_1 \frac{\partial \phi_t}{\partial s_1}, \\ D_{21} &= \frac{\partial V_1}{\partial s_2} - V_2 \frac{\partial \phi_t}{\partial s_2}, \quad D_{22} = \frac{\partial V_2}{\partial s_2} + V_1 \frac{\partial \phi_t}{\partial s_2}. \end{aligned}\right\} \tag{2.5b}$$

(We note in passing that the fibre rotation rate $\dot{\phi}_t = \dot{\phi}$ is given by $\dot{\phi}_t = D_{12}$.) In analogous fashion, the spatial gradient of the virtual displacement is $\mathbf{W} \equiv \hat{\nabla}\delta\mathbf{u} = W_{ij}\boldsymbol{\varepsilon}_i\boldsymbol{\varepsilon}_j$ where

$$\left.\begin{aligned} W_{11} &= \frac{\partial \delta U_1}{\partial s_1} - \delta U_2 \frac{\partial \phi_t}{\partial s_1}, \quad W_{12} = \frac{\partial \delta U_2}{\partial s_1} + \delta U_1 \frac{\partial \phi_t}{\partial s_1}, \\ W_{21} &= \frac{\partial \delta U_1}{\partial s_2} - \delta U_2 \frac{\partial \phi_t}{\partial s_2}, \quad W_{22} = \frac{\partial \delta U_2}{\partial s_2} + \delta U_1 \frac{\partial \phi_t}{\partial s_2}. \end{aligned}\right\} \tag{2.6}$$

2.2. *Equilibrium*

Consider a homogeneous Cosserat medium subjected to a distribution of Cauchy stress $\boldsymbol{\sigma}$ and a couple stress per unit area $\mathbf{m}$. We limit attention to the two-dimensional case and again we take as axes the orthogonal curvilinear co-ordinate system (ξ_1, ξ_2), as shown in Figs 1 and 2. The third co-ordinate ξ_3 is taken to be orthogonal to the ξ_1- and ξ_2-directions, and forms a right-handed triad with the ξ_1 and ξ_2 co-ordinates. Since in-plane deformations are considered we can take $\xi_3 = X_3 = x_3$.

Force equilibrium gives

$$\hat{\nabla} \cdot \boldsymbol{\sigma} = \mathbf{0} \tag{2.7}$$

or, in terms of physical components,

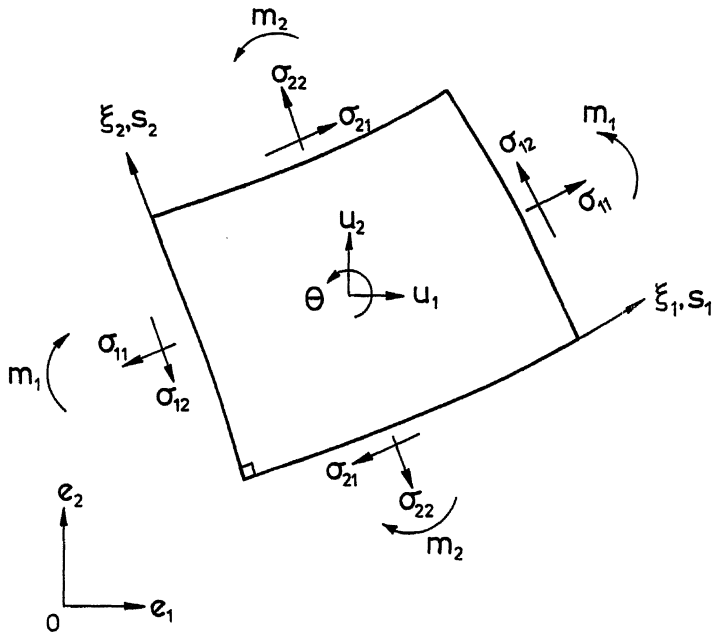

Fig. 2. Two-dimensional stress state at a material point in a Cosserat medium.

$$\frac{\partial \sigma_{11}}{\partial s_1} - (\sigma_{12} + \sigma_{21}) \frac{\partial \phi_t}{\partial s_1} + \frac{\partial \sigma_{21}}{\partial s_2} + (\sigma_{11} - \sigma_{22}) \frac{\partial \phi_t}{\partial s_2} = 0 \tag{2.8a}$$

and

$$\frac{\partial \sigma_{12}}{\partial s_1} + (\sigma_{11} - \sigma_{22}) \frac{\partial \phi_t}{\partial s_1} + \frac{\partial \sigma_{22}}{\partial s_2} + (\sigma_{12} + \sigma_{21}) \frac{\partial \phi_t}{\partial s_2} = 0. \tag{2.8b}$$

We specialise the theory to the case of unidirectional fibre composites, and assume that the bending moment per unit area in the fibre direction m_1 is finite, while the bending moment in the transverse direction m_2 vanishes (see Fig. 2). Moment equilibrium within the body implies

$$\sigma_{21} - \sigma_{12} = \frac{\partial m_1}{\partial s_1} + m_1 \frac{\partial \phi_t}{\partial s_2}. \tag{2.9}$$

On the surface of the deformed body, we have

$$n_i \sigma_{ij} = T_j, \quad \text{and} \quad n_1 m_1 = Q \tag{2.10}$$

where $\mathbf{n}$ is the unit normal, $\mathbf{T}$ is the surface force traction per unit area and $\mathbf{Q} = Q\mathbf{e}_3$ is the surface moment traction per unit area.

2.3. *Principle of virtual work*

Consider a two-dimensional problem of a Cosserat solid in a planar domain Ω with boundary surface S. The principle of virtual work (with $m_2 = 0$) states

$$\int_\Omega [\sigma_{ij}\delta\gamma_{ji} + m_1\delta\kappa_1]\,\mathrm{d}\Omega = \int_S [T_j\delta U_j + Q\delta\theta]\,\mathrm{d}S \tag{2.11}$$

where the virtual strain $\delta\boldsymbol{\gamma} = \delta\gamma_{ij}\mathbf{e}_i\mathbf{e}_j$ is defined by

$$\delta\gamma_{ij} \equiv W_{ji} + \varepsilon_{ij}\delta\theta \tag{2.12}$$

and the component $\delta\kappa_1$ of the virtual curvature is

$$\delta\kappa_1 \equiv \frac{\partial\delta\theta}{\partial s_1}. \tag{2.13}$$

Here, ε_{ij} is the two-dimensional permutation symbol and is defined by $\varepsilon_{12} = 1, \varepsilon_{21} = -1$ and $\varepsilon_{ij} = 0$ otherwise.

For the limiting case of a conventional non-Cosserat solid, couple stresses vanish and $\delta\theta$ satisfies

$$\delta\theta = \tfrac{1}{2}(W_{12} - W_{21}). \tag{2.14}$$

Then, $\delta\boldsymbol{\gamma}$ reduces to the virtual increment of the Eulerian strain $\delta\mathbf{E}$,

$$\delta\gamma_{ij} = \delta E_{ij} = \tfrac{1}{2}(W_{ji} + W_{ij}) \tag{2.15}$$

and the principle of virtual work attains the familiar form

$$\int_\Omega \sigma_{ij}\delta E_{ij}\,\mathrm{d}\Omega = \int_S T_j\delta U_j\,\mathrm{d}S. \tag{2.16}$$

3. UNIT CELL ANALYSIS

At the macroscopic scale, we assume the fibre composite behaves as a "smeared-out" homogeneous solid. In order to derive the governing kinematic, equilibrium and constitutive relations for the "smeared-out" fibre composite, we consider the response of a unit cell *micro-medium* surrounding a macroscopic point (ξ_1, ξ_2) in the "smeared-out" composite, as shown in Fig. 3(a). First, we give the geometry and some notation for micro-medium. The unit cell is of physical height $\mathrm{d}s_2$ and the top and bottom faces are bounded by two ξ_2 contours. Similarly, the unit cell is of physical length $\mathrm{d}s_1$ and the ends are bounded by two ξ_1 contours. At the microscopic scale of $\mathrm{d}s_1$ and $\mathrm{d}s_2$, the unit cell contains fibre material of volume fraction c and height $h_\mathrm{f} = c\,\mathrm{d}s_2$, and matrix material of volume fraction $(1-c)$ and height $h_\mathrm{m} = (1-c)\,\mathrm{d}s_2$, as shown in Fig. 3(b). The actual fibre diameter d enters the formulation at the constitutive level in Section 4 below. We use a subscript f or a superscript f to denote the fibres and a subscript m or a superscript m to denote the matrix. Both the fibre material and the matrix material are assumed to behave as classical non-Cosserat media: on the length scale of the micro-medium they do not support couple stress.

Following the strategy of Mindlin (1964), we use micro curvilinear co-ordinates (η_1, η_2) to define a microscopic material point within the unit cell. The co-ordinates (η_1, η_2) are centred at any macroscopic point of interest (ξ_1, ξ_2) and are locally parallel

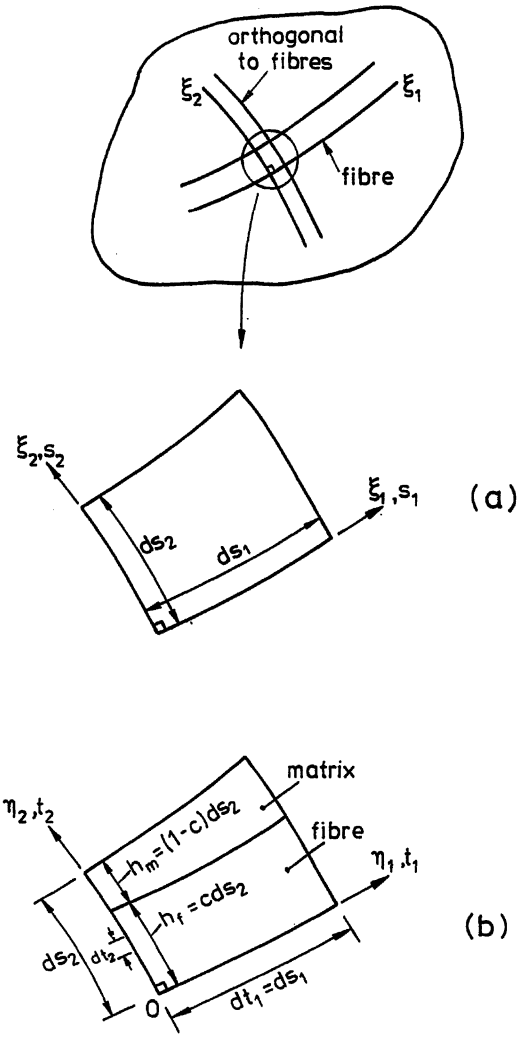

Fig. 3. (a) A unit cell micro medium in the "smeared-out" composite drawn in the deformed configuration; (b) the composition of the unit cell and the local micro co-ordinates.

to the (ξ_1, ξ_2) co-ordinates as shown in Fig. 3(b). Physical distance along the η_1-direction is designated t_1, and physical distance along the η_2-direction is designated t_2. We shall assume that the microstructure does not vary along the η_1-direction, and we thereby take $\eta_1 = \xi_1$ and $t_1 = s_1$. The microstructure does vary along the η_2-direction, and so it is necessary to distinguish between η_2 and ξ_2, and between t_2 and s_2. Quantities with a circumflex (^) and with either a subscript f or a superscript f represent averages over the height of the fibre layer of the unit cell; similarly, quantities with a circumflex (^) and with either a subscript m or a superscript m represent averages over the height of the matrix layer of the unit cell. Quantities with a circumflex (^) but without subscript or superscript labels f or m denote averages over the height of the whole unit cell.

Now consider the deformation state within the unit cell of physical dimension ds_1 by ds_2. The fibre material is represented by a Timoshenko beam and deforms in both axial extension and in bending; the beam also suffers a uniform in-plane sliding shear

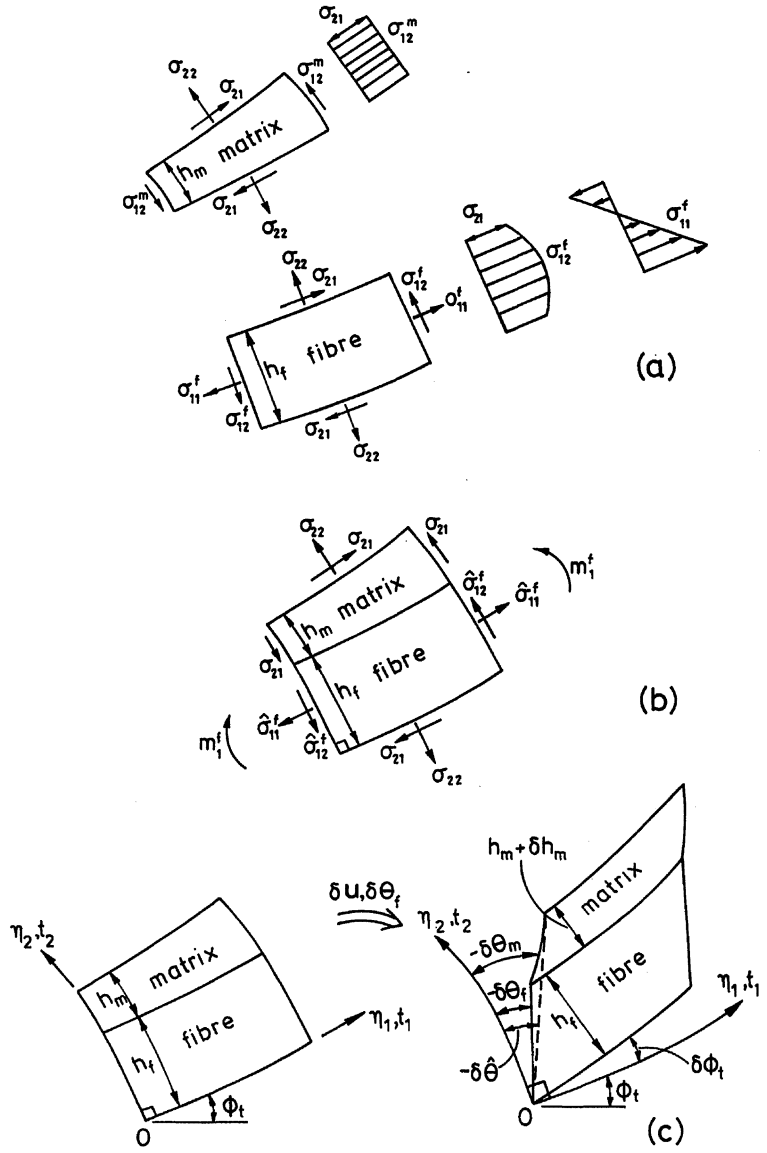

Fig. 4. (a) Stress state within the unit cell; (b) the work-equivalent stresses and couple stress of the unit cell; (c) the unit cell in the deformed configuration subjected to a virtual displacement field $\delta\mathbf{u}$ and an independent virtual rotation field $\delta\theta_f$.

strain in the η_1-direction, and is inextensible in the transverse t_2-direction. The stress state within the Timoshenko beam of the fibre material is sketched in Fig. 4(a). The top and bottom faces of the beam are subjected to equal shear tractions σ_{21} and to equal normal tractions σ_{22}. A direct stress component σ^f_{11} varies linearly with depth t_2 and gives rise to a bending moment and an axial force at the ends of the beam. Similarly, the transverse shear force on the beam cross-section is the resultant of the shear stress σ^f_{12} which varies quadratically with depth t_2.

The matrix material within the unit cell also deforms as a Timoshenko beam. Additionally, the matrix undergoes uniform transverse straining. Since the matrix is much more compliant than the fibres, we neglect the axial stress σ^m_{11} within the matrix

and assume the matrix is subjected to a uniform transverse normal stress σ_{22} and to a uniform shear stress $\sigma_{12}^{m} = \sigma_{21}$ as shown in Fig. 4(a).

To proceed, we develop kinematic and virtual work relations for the fibre material and the matrix material within the unit cell. A virtual work statement for the unit cell enables us to relate the stress state within the unit cell to a macroscopic Cosserat framework.

Virtual work for fibre material in the unit cell. The fibre material is assumed to behave as a Timoshenko beam subjected to bending, longitudinal stretching and transverse shear, but without transverse stretching. The beam is aligned with the η_1 co-ordinate, and is inclined at an angle ϕ_t to the x_1-direction. Since the fibres are parallel sided in the undeformed configuration and suffer vanishing transverse strain, we have $\partial\phi_t/\partial t_2 = 0$. For the Timoshenko beam, the pointwise virtual displacements are taken as

$$\delta U_1(\eta_1, \eta_2) = \delta\hat{U}_{1f}(\xi_1, \xi_2) - (t_2 - \tfrac{1}{2}h_f)\delta\theta_f(\xi_1, \xi_2),$$
$$\delta U_2(\eta_1, \eta_2) = \delta\hat{U}_{2f}(\xi_1, \xi_2) \tag{3.1}$$

where the angle θ_f is the rotation of the fibre cross-section from the initial, stress-free configuration. In compliance with Timoshenko beam theory, θ_f is in general different from the rotation of the neutral axis of the beam. At a typical microscopic point in the fibre material, the pointwise virtual Eulerian strain $\delta\mathbf{E}$ follows from relations (2.6) and (2.15) expressed in the micro co-ordinates (η_1, η_2), giving

$$\delta E_{11} = \frac{\partial\delta\hat{U}_{1f}}{\partial s_1} - \delta\hat{U}_{2f}\frac{\partial\phi_t}{\partial s_1} - (t_2 - \tfrac{1}{2}h_f)\frac{\partial\delta\theta_f}{\partial s_1}, \tag{3.2a}$$

$$\delta E_{12} = \frac{1}{2}\left(\frac{\partial\delta\hat{U}_{2f}}{\partial s_1} - \delta\theta_f + \delta U_1\frac{\partial\phi_t}{\partial s_1}\right), \tag{3.2b}$$

and

$$\delta E_{22} = 0. \tag{3.2c}$$

The internal virtual work δw_f of the fibre material over a volume $\mathrm{d}s_1 h_f$ is

$$\delta w_f = \int_0^{ds_1}\int_0^{h_f} [\sigma_{11}^f\delta E_{11} + \sigma_{22}\delta E_{22} + 2\sigma_{12}^f\delta E_{12}]\,\mathrm{d}t_2\,\mathrm{d}t_1$$
$$= c\left\{\hat{\sigma}_{11}^f\left(\frac{\partial\delta\hat{U}_{1f}}{\partial s_1} - \delta\hat{U}_{2f}\frac{\partial\phi_t}{\partial s_1}\right) + m_1^f\frac{\partial\delta\theta_f}{\partial s_1}\right.$$
$$\left. + \hat{\sigma}_{12}^f\left(\frac{\partial\delta\hat{U}_{2f}}{\partial s_1} + \delta\hat{U}_{1f}\frac{\partial\phi_t}{\partial s_1} - \delta\theta_f\right)\right\}\mathrm{d}s_1\,\mathrm{d}s_2 \tag{3.3a}$$

where

$$\hat{\sigma}^{\mathrm{f}}_{11} = \frac{1}{h_{\mathrm{f}}}\int_0^{h_{\mathrm{f}}} \sigma^{\mathrm{f}}_{11}\,\mathrm{d}t_2,$$

$$\hat{\sigma}^{\mathrm{f}}_{12} = \frac{1}{h_{\mathrm{f}}}\int_0^{h_{\mathrm{f}}} \sigma^{\mathrm{f}}_{12}\,\mathrm{d}t_2,$$

$$m^{\mathrm{f}}_1 = \frac{1}{h_{\mathrm{f}}}\int_0^{h_{\mathrm{f}}} -(t_2 - h_{\mathrm{f}}/2)\sigma^{\mathrm{f}}_{11}\,\mathrm{d}t_2 \tag{3.3b}$$

are the average stresses and couple stress taken over the height of the fibre [see Fig. 4(b)]. In the integration of the term $2\sigma^{\mathrm{f}}_{12}\delta E_{12}$ in (3.3a) the pointwise virtual displacement δU_1 appearing in δE_{12} is replaced by $\delta \hat{U}_{1\mathrm{f}}$. This can be justified as a *first order approximation* valid for an infinitesimal unit cell. It is clear from (3.3a) that the average stress measures $\hat{\sigma}^{\mathrm{f}}_{11}, m^{\mathrm{f}}_1$ and $\hat{\sigma}^{\mathrm{f}}_{12}$ are work-equivalent to the stress distributions σ^{f}_{11} and σ^{f}_{12}. Equation (3.3a) can be simplified further to

$$\delta w_{\mathrm{f}} = c\left\{\hat{\sigma}^{\mathrm{f}}_{11}\left(\frac{\partial \delta \hat{U}_1}{\partial s_1} - \delta \hat{U}_2 \frac{\partial \hat{\phi}_{\mathrm{t}}}{\partial s_1}\right) + m^{\mathrm{f}}_1 \frac{\partial \delta \theta_{\mathrm{f}}}{\partial s_1} + \hat{\sigma}^{\mathrm{f}}_{12}\left(\frac{\partial \delta \hat{U}_2}{\partial s_1} + \delta \hat{U}_1 \frac{\partial \hat{\phi}_{\mathrm{t}}}{\partial s_1} - \delta \theta_{\mathrm{f}}\right)\right\} \mathrm{d}s_1\,\mathrm{d}s_2. \tag{3.4}$$

In the reduction of (3.3a) to (3.4) we use the following first order approximations for the pointwise virtual displacement δU_i and the fibre misalignment angle ϕ_{t} at the microscopic level within the fibre

$$|\delta U_i - \delta \hat{U}_i| \ll |\delta \hat{U}_i|, \quad \left|\frac{\partial \delta U_i}{\partial s_1} - \frac{\partial \delta \hat{U}_i}{\partial s_1}\right| \ll \left|\frac{\partial \delta \hat{U}_i}{\partial s_1}\right| \quad \text{for } i = 1, 2 \tag{3.5a}$$

and

$$|\phi_{\mathrm{t}} - \hat{\phi}_{\mathrm{t}}| \ll |\hat{\phi}_{\mathrm{t}}|, \quad \left|\frac{\partial \phi_{\mathrm{t}}}{\partial s_1} - \frac{\partial \hat{\phi}_{\mathrm{t}}}{\partial s_1}\right| \ll \left|\frac{\partial \hat{\phi}_{\mathrm{t}}}{\partial s_1}\right|. \tag{3.5b}$$

Relations (3.5a) and (3.5b) are justified by taking the unit cell to be sufficiently small. Upon replacing the average virtual displacements within the fibre by the average virtual displacements of the whole unit cell, one arrives at (3.4). A similar first order approximation will be applied for the matrix material of the unit cell as follows.

Virtual work for matrix material in the unit cell. It is assumed that the matrix in the unit cell is subjected to transverse normal stress and sliding shear stress as shown in Fig. 4(b). We neglect the longitudinal component of stress in the matrix on the basis that the Young's modulus of the fibres is much greater than that of the matrix. The pointwise virtual displacements of a microscopic point within the matrix are taken as

$$\delta U_1(\eta_1, \eta_2) = \delta \hat{U}_{1\mathrm{m}}(\xi_1, \xi_2) - (t_2 - h_{\mathrm{f}} - \tfrac{1}{2}h_{\mathrm{m}})\delta\theta_{\mathrm{m}}(\xi_1, \xi_2),$$

$$\delta U_2(\eta_1, \eta_2) = \delta \hat{U}_{2\mathrm{m}}(\xi_1, \xi_2) + (t_2 - h_{\mathrm{f}} - \tfrac{1}{2}h_{\mathrm{m}})\frac{\partial \delta U_2(\eta_1, \eta_2)}{\partial t_2} \tag{3.6}$$

where θ_m is the rotation of the cross-section of the matrix layer. We shall assume that $\partial\delta U_2(\eta_1,\eta_2)/\partial t_2$ is independent of the micro co-ordinate η_2 within the matrix microvolume. Then, since the fibre in the unit cell is assumed to be transversely inextensible we may write

$$\frac{\partial\delta U_2}{\partial t_2}=\frac{1}{1-c}\frac{\partial\delta\hat{U}_2}{\partial s_2}. \tag{3.7a}$$

Similarly, because the inclination ϕ_t of the fibre is taken to be independent of t_2 within the fibre microvolume, the gradient of ϕ_t within the matrix is related to the average value within the whole unit cell by

$$\frac{\partial\phi_t}{\partial t_2}=\frac{1}{1-c}\frac{\partial\hat{\phi}_t}{\partial s_2}. \tag{3.7b}$$

By making use of (2.6) and (2.15) in the micro co-ordinates (η_1, η_2), the pointwise virtual Eulerian strain within the matrix is

$$\delta E_{11}=\frac{\partial\delta\hat{U}_{1m}}{\partial s_1}-\delta U_2\frac{\partial\phi_t}{\partial s_1}-(t_2-h_f-\tfrac{1}{2}h_m)\frac{\partial\delta\theta_m}{\partial s_1}, \tag{3.8a}$$

$$\delta E_{12}=\frac{1}{2}\left(\frac{\partial\delta U_2}{\partial s_1}+\delta U_1\frac{\partial\phi_t}{\partial s_1}-\delta\theta_m-\delta U_2\frac{\partial\phi_t}{\partial t_2}\right), \tag{3.8b}$$

$$\delta E_{22}=\frac{\partial\delta U_2}{\partial t_2}+\delta U_1\frac{\partial\phi_t}{\partial t_2}. \tag{3.8c}$$

The virtual Eulerian strain of the matrix can be written in terms of the average displacements of the whole unit cell upon making use of (3.7a) and (3.7b), and the first order approximations (3.5); the resulting simplified form is

$$\delta E_{11}\approx\frac{\partial\delta\hat{U}_1}{\partial s_1}-\delta\hat{U}_2\frac{\partial\hat{\phi}_t}{\partial s_1}-(t_2-h_f-\tfrac{1}{2}h_m)\frac{\partial\delta\theta_m}{\partial s_1}, \tag{3.9a}$$

$$\delta E_{12}\approx\frac{1}{2}\left(\frac{\partial\delta\hat{U}_2}{\partial s_1}+\delta\hat{U}_1\frac{\partial\hat{\phi}_t}{\partial s_1}-\delta\theta_m-\delta\hat{U}_2\frac{1}{1-c}\frac{\partial\hat{\phi}_t}{\partial s_2}\right), \tag{3.9b}$$

$$\delta E_{22}\approx\frac{1}{1-c}\frac{\partial\delta\hat{U}_2}{\partial s_2}+\delta\hat{U}_1\frac{1}{1-c}\frac{\partial\hat{\phi}_t}{\partial s_2}. \tag{3.9c}$$

Note that δE_{12} and δE_{22} are independent of the local physical distance t_2. The internal virtual work for the matrix portion of the unit cell δw_m is obtained by substituting relations (3.9b)–(3.9c) into (2.16) and by neglecting the contribution of σ_{11}. This gives

$$\delta w_m=\int_0^{ds_1}\int_{h_f}^{h_f+h_m}(\sigma_{22}\delta E_{22}+2\sigma_{12}^m\delta E_{12})\,dt_2\,dt_1$$

$$\approx\left\{\sigma_{22}\left(\frac{\partial\delta\hat{U}_2}{\partial s_2}+\delta\hat{U}_1\frac{\partial\hat{\phi}_t}{\partial s_2}\right)-\sigma_{21}\delta\hat{U}_2\frac{\partial\hat{\phi}_t}{\partial s_2}\right.$$

$$+(1-c)\sigma_{21}\left(\frac{\partial\delta\hat{U}_2}{\partial s_1}+\delta\hat{U}_1\frac{\partial\hat{\phi}_t}{\partial s_1}-\delta\theta_m\right)\Bigg\}ds_1 ds_2. \tag{3.10}$$

Virtual work for the smeared-out homogeneous composite. The internal virtual work over a volume $ds_1 ds_2$ of the unit cell of the composite is obtained by adding (3.4) and (3.10). Upon making use of the following averaging relations

$$c\delta\theta_f+(1-c)\delta\theta_m=\delta\hat{\theta}=-\frac{\partial\delta\hat{U}_1}{\partial s_2}, \tag{3.11}$$

$$c\sigma_{12}^f+(1-c)\sigma_{21}=\hat{\sigma}_{12}, \tag{3.12}$$

and

$$c\hat{\sigma}_{11}^f=\hat{\sigma}_{11},\quad cm_1^f=m_1, \tag{3.13}$$

the internal work is

$$\delta w=\{\hat{\sigma}_{11}\hat{W}_{11}+\sigma_{22}\hat{W}_{22}+\hat{\sigma}_{12}(\hat{W}_{12}-\delta\theta_f)+\sigma_{21}(\hat{W}_{21}+\delta\theta_f)+m_1\delta\kappa_1\}ds_1 ds_2 \tag{3.14}$$

where $\hat{W}_{ij}$ is defined by (2.6) and the virtual curvature $\delta\kappa_1$ is defined by (2.13). Each of the quantities in relation (3.14) are functions of macro co-ordinates (ξ_1, ξ_2). Now consider the composite to be "smeared-out" and reinterpret (3.14) as the internal virtual work over a micro-volume of $ds_1 ds_2$ of the "smeared-out" homogeneous composite. This homogeneous composite is subjected to a stress state of $\sigma_{11}\equiv\hat{\sigma}_{11}$, σ_{22}, $\sigma_{12}\equiv\hat{\sigma}_{12}$, σ_{21} and couple stress m_1, and undergoes a displacement $U_i\equiv\hat{U}_i$ and an independent rotation $\theta\equiv\theta_f$. We integrate the virtual work relation (3.14) over the total volume Ω of the composite and use the divergence theorem to derive the principle of virtual work for the "smeared-out" composite:

$$\int_\Omega\{\sigma_{11}W_{11}+\sigma_{22}W_{22}+\sigma_{12}(W_{12}-\delta\theta_f)+\sigma_{21}(W_{21}+\delta\theta_f)+m_1\delta\kappa_1\}\,d\Omega$$

$$=\int_S(T_1\delta U_1+T_2\delta U_2+Q\delta\theta_f)\,dS \tag{3.15}$$

provided that the stresses and the couple stress satisfy the equilibrium equations (2.8)–(2.10). Here, T_i is the force traction and Q is the torque traction acting on the surface S of the domain Ω. It can be seen that (3.15) is identical to the principle of virtual work for a general Cosserat solid, as given by (2.11). Henceforth, we shall treat the composite as an equivalent Cosserat solid. The above unit cell analysis enables us to identify the rotation angle of the fibre cross-sectional area θ_f with the *independent micro rotation angle* θ in the Cosserat theory. It also provides a guideline for stipulation of the constitutive law for the composite in Section 4.

3.1. *Rate form of principle of virtual work*

We require a rate form of the principle of virtual work for two reasons:

(i) the equilibrium path is strongly unstable with a snap-back behaviour at the maximum load. In order to calculate the equilibrium path a modified Rik's algorithm (Crisfield, 1991) is used: this requires calculation of the current tangent stiffness matrix;
(ii) the flow-theory constitutive law for the composite is given in incremental form in Section 4 below.

In order to obtain the virtual work statement in rate form we rewrite the principle of virtual work in terms of the undeformed, reference configuration as

$$\int_{\Omega_0} J\{\sigma_{ij}(W_{ij}+\varepsilon_{ji}\delta\theta_f)+m_1\delta\kappa_1\}\,d\Omega_0 = \int_{S_0}(t_j\delta u_j+q\delta\theta_f)\,dS_0 \tag{3.16}$$

where the subscript 0 indicates the undeformed configuration. The Jacobian of deformation J is $J = d\Omega/d\Omega_0$, and the nominal traction t_j and nominal moment q are defined by

$$t_j\mathbf{e}_j\,dS_0 = T_j\boldsymbol{\varepsilon}_j\,dS, \quad q\,dS_0 = Q\,dS. \tag{3.17}$$

Note that the internal virtual work expression is phrased in terms of physical components in the deformed curvi-linear co-ordinate system, and the external virtual work is written in terms of Cartesian co-ordinates in the undeformed configuration.

To derive the rate form of the principle of virtual work, we take the material time derivative D/Dt of (3.16), giving

$$\int_{\Omega_0} J\{(\dot\sigma_{ij}+\sigma_{ij}\dot J/J)(W_{ij}+\varepsilon_{ji}\delta\theta_f)+\sigma_{ij}(DW_{ij}/Dt+\varepsilon_{ji}\delta\dot\theta_f)+(\dot m_1+m_1\dot J/J)\delta\kappa_1$$

$$+m_1D\delta\kappa_1/Dt\}\,d\Omega_0 = \int_{S_0}(\dot t_j\delta u_j+t_j\delta\dot u_j+\dot q\delta\theta_f+q\delta\dot\theta_f)\,dS_0. \tag{3.18}$$

The above relation is re-phrased in a more convenient form as follows. First note that $\dot J/J = D_{kk}$. Next, denote the spatial gradient in the deformed configuration of the velocity increment $\delta\mathbf{v}$ by $\mathbf{C} \equiv \vec{\nabla}\delta\mathbf{v} = C_{ij}\boldsymbol{\varepsilon}_i\boldsymbol{\varepsilon}_j$. We can express the material time derivative of W_{ij} in the form

$$\frac{DW_{ij}}{Dt} = C_{ij}-(W_{ik}\varepsilon_{kj}+W_{kj}\varepsilon_{ki})\dot\phi_t-D_{ik}W_{kj} \tag{3.19}$$

by the following argument. The tensor

$$\frac{D\mathbf{W}}{Dt} \equiv \frac{D}{Dt}(\vec{\nabla}\delta\mathbf{u}) = \mathbf{C}-\mathbf{D}\cdot\mathbf{W} \tag{3.20}$$

can be rewritten in terms of the curvilinear base vectors $(\boldsymbol{\varepsilon}_1, \boldsymbol{\varepsilon}_2)$ as

$$\frac{D\mathbf{W}}{Dt} = (C_{ij} - D_{ik}W_{kj})\boldsymbol{\varepsilon}_i\boldsymbol{\varepsilon}_j. \tag{3.21}$$

Alternatively, $D\mathbf{W}/Dt$ can be written as

$$\frac{D\mathbf{W}}{Dt} = \frac{D}{Dt}(W_{ij}\boldsymbol{\varepsilon}_i\boldsymbol{\varepsilon}_j) = \frac{DW_{ij}}{Dt}\boldsymbol{\varepsilon}_i\boldsymbol{\varepsilon}_j + W_{ij}(\boldsymbol{\varepsilon}_i\dot{\boldsymbol{\varepsilon}}_j + \dot{\boldsymbol{\varepsilon}}_i\boldsymbol{\varepsilon}_j) \tag{3.22}$$

or, upon making use of $\dot{\boldsymbol{\varepsilon}}_i = \dot{\phi}_t\varepsilon_{ij}\boldsymbol{\varepsilon}_j$, as

$$\frac{D\mathbf{W}}{Dt} = \frac{DW_{ij}}{Dt}\boldsymbol{\varepsilon}_i\boldsymbol{\varepsilon}_j + (W_{ik}\varepsilon_{kj} + W_{kj}\varepsilon_{ki})\dot{\phi}_t\boldsymbol{\varepsilon}_i\boldsymbol{\varepsilon}_j. \tag{3.23}$$

Now equate (3.21) and (3.23) to get (3.19).

The material time derivative of the curvature increment is written as

$$\frac{D\delta\kappa_1}{Dt} = \delta\dot{\kappa}_1 - D_{11}\delta\kappa_1 \tag{3.24}$$

where the curvature rate and virtual curvature rate are defined by

$$\dot{\kappa}_1 = \frac{\partial\dot{\theta}_f}{\partial s_1}, \quad \delta\dot{\kappa}_1 = \frac{\partial\delta\dot{\theta}_f}{\partial s_1}. \tag{3.25}$$

Finally, we make use of the principle of virtual work (3.15), but written in the form

$$\int_{\Omega_0} J\{\sigma_{ij}(C_{ij} + \varepsilon_{ji}\delta\dot{\theta}_f) + m_1\delta\dot{\kappa}_1\}\,\mathrm{d}\Omega_0 = \int_{S_0} (t_j\delta v_j + q\delta\dot{\theta}_f)\,\mathrm{d}S_0 \tag{3.26}$$

and substitute relations (3.19), (3.24) and (3.26) into (3.18) in order to obtain a convenient rate form of virtual work:

$$\int_{\Omega_0} J\{(\dot{\sigma}_{ij} + \sigma_{ij}D_{kk} + \sigma_{kj}\varepsilon_{ki}\dot{\phi}_t + \sigma_{ik}\varepsilon_{kj}\dot{\phi}_t - \sigma_{kj}D_{ki})W_{ij} + (\dot{\sigma}_{ij} + \sigma_{ij}D_{kk})\varepsilon_{ji}\delta\theta_f$$

$$+ (\dot{m}_1 + m_1D_{22})\delta\kappa_1\}\,\mathrm{d}\Omega_0 = \int_{S_0} (\dot{t}_j\delta u_j + \dot{q}\delta\theta_f)\,\mathrm{d}S_0. \tag{3.27}$$

4. CONSTITUTIVE LAW

We shall present the constitutive law in terms of physical components of stress and strain in the deformed curvi-linear reference frame. The constitutive law of the composite is based on the plasticity law given by Slaughter *et al.* (1993) and by Fleck *et al.* (1995). The bending resistance of the composite is calculated by neglecting the matrix contribution to couple stresses. Simple beam theory for circular fibres of diameter d, axial modulus E_f and volume fraction c gives the relation between the couple stress m_1 in the composite and the associated curvature κ_1; in rate form this appears as

$$\dot{m}_1 = \frac{cE_f d^2}{16}\dot{\kappa}_1. \tag{4.1}$$

The "smeared-out" composite is ascribed a longitudinal Young's modulus $E_L = cE_f$, and deformation in the fibre direction is taken to be elastic such that

$$\dot{\sigma}_{11} = E_L D_{11}. \tag{4.2}$$

In order to estimate the sliding and transverse shear responses we refer to the unit cell construction of Fig. 4(c). The transverse shear stress rate $\dot{\sigma}_{12}$ of the composite is related to the velocity gradient and rotation rate of the fibre cross-section by

$$\dot{\sigma}_{12} = c\dot{\sigma}^f_{12} + (1-c)\dot{\sigma}_{21}, \quad \dot{\sigma}^f_{12} = G_f(D_{12} - \dot{\theta}_f) \tag{4.3}$$

where it is assumed that the sliding shear stress rate $\dot{\sigma}_{21}$ is exerted on both the matrix and the fibres. G_f is the shear modulus of the fibres. The sliding shear strain rate $\dot{\gamma}_s$ and the transverse strain rate $\dot{\varepsilon}_T$ of the composite are given by

$$\dot{\gamma}_s = D_{12} + D_{21} \tag{4.4}$$

and

$$\dot{\varepsilon}_T = D_{22}. \tag{4.5}$$

The combined sliding shear and transverse response of the composite is taken to be that of an elastic–plastic flow theory solid, which parallels the deformation theory description of Budiansky and Fleck (1993, 1994). They propose an effective shear stress τ_e defined by

$$\tau_e = \sqrt{\sigma_{21}^2 + \frac{\sigma_{22}^2}{R^2}} \tag{4.6}$$

where the constant R is interpreted as the ratio of yield strength in transverse tension to that in shear. The sliding shear strain rate $\dot{\gamma}_s$ is decomposed into an elastic part $\dot{\sigma}_{21}/G$ and a plastic part $\dot{\gamma}^p_s$; similarly the transverse strain rate $\dot{\varepsilon}_T$ can be decomposed into an elastic part $\dot{\sigma}_{22}/E_T$ and a plastic part $\dot{\varepsilon}^p_T$. We assume that the plastic strain rate vector $(\dot{\gamma}^p_s, \dot{\varepsilon}^p_T)$ is normal to the yield surface in the $(\sigma_{22}, \sigma_{21})$ space, giving

$$\dot{\gamma}^p_s = \dot{\gamma}_e \partial\tau_e/\partial\sigma_{21}, \quad \text{and} \quad \dot{\varepsilon}^p_T = \dot{\gamma}_e \partial\tau_e/\partial\sigma_{22} \tag{4.7}$$

where the effective strain rate $\dot{\gamma}_e$ is defined by the work equivalent statement

$$\tau_e\dot{\gamma}_e = \sigma_{21}\dot{\gamma}^p_s + \sigma_{22}\dot{\varepsilon}^p_T \tag{4.8}$$

and is related to $(\dot{\gamma}^p_s, \dot{\varepsilon}^p_T)$ by

$$\dot{\gamma}_e = \sqrt{(\dot{\gamma}^p_s)^2 + R^2(\dot{\varepsilon}^p_T)^2}. \tag{4.9}$$

It remains to state a strain hardening law to link τ_e and γ_e. The functional dependence of γ_e upon τ_e is assumed to equal that of γ^p_s on τ for the composite in pure shear, so that

$$\gamma_e = \left[\frac{1}{G_s(\tau_e)} - \frac{1}{G}\right]\tau_e \tag{4.10}$$

where $G_s(\tau)$ denotes the secant shear modulus of the shear stress τ versus total shear strain γ curve. G is the elastic shear modulus of the composite. In rate form, (4.10) becomes

$$\dot{\gamma}_e = \dot{\tau}_e / H(\tau_e) \tag{4.11}$$

where the hardening modulus H is related to G_s by

$$\frac{1}{H} = \frac{1}{G_s} - \frac{\tau_e}{G_s^2}\frac{dG_s}{d\tau_e} - \frac{1}{G}. \tag{4.12}$$

A Ramberg–Osgood description is used for the strain hardening response

$$\frac{\gamma_e}{\gamma_Y} = \frac{\tau_e}{\tau_Y} + \alpha\left(\frac{\tau_e}{\tau_Y}\right)^n, \quad G = \frac{\tau_Y}{\gamma_Y}, \tag{4.13}$$

where α is given the value 3/7 and (τ_Y, γ_Y, n) are material constants for the composite. Then, the hardening modulus H is

$$H = \frac{\partial \tau_e}{\partial \gamma_e} = \frac{G}{\alpha n}\left(\frac{\tau_Y}{\tau_e}\right)^{n-1} \quad \text{if } \dot{\tau}_e > 0 \tag{4.14}$$

and $H = \infty$ if $\dot{\tau}_e \leqslant 0$. Inversion of the above stress–strain relations for combined sliding shear and transverse loading gives

$$\left.\begin{aligned} \dot{\sigma}_{22} &= \left(E_T - \frac{G^2}{G+H}\frac{\sigma_{22}^2}{\tau_e^2}\right)\dot{\varepsilon}_T - \frac{G^2}{G+H}\frac{\sigma_{21}\sigma_{22}}{\tau_e^2}\dot{\gamma}_S, \\ \dot{\sigma}_{21} &= -\frac{G^2}{G+H}\frac{\sigma_{21}\sigma_{22}}{\tau_e^2}\dot{\varepsilon}_T + \left(G - \frac{G^2}{G+H}\frac{\sigma_{22}^2}{\tau_e^2}\right)\dot{\gamma}_S. \end{aligned}\right\} \tag{4.15}$$

Finally, we specialise the constitutive description by setting $E_T = R^2 G$; consequently, for proportional loading, the elastic–plastic response simplifies to $\gamma_s = \sigma_{21}/G_s$ and $\varepsilon_T = \sigma_{22}/R^2 G_s$, as discussed by Slaughter *et al.* (1993).

Specification of the composite properties. We focus on the compressive strength of unidirectional carbon fibre reinforced epoxy. Unless otherwise stated we shall assume a uniform volume fraction $c = 0.6$, and take $E_L/\tau_y = 2500$. The shear modulus of the fibres is taken to be $G_f/\tau_y = 400$ and the shear modulus of the composite is $G/\tau_y = 1/\gamma_y = 100$. The transverse modulus of the composite is $E_T/\tau_y = 250$, giving $R^2 = E_T/G = 2.5$. The strain hardening index n is taken to lie in the range 3–19.

5. APPLICATION OF CONSTITUTIVE FRAMEWORK TO FIBRE MICROBUCKLING

A finite strain Lagrangian-based finite element code has been developed from the couple stress formulation of the previous sections. The details of the finite element implementation are presented in Appendix B. As a check on the formulation and programming of the finite element code, we consider first the simplified geometry of an infinite band of misalignment and compare the results with those given previously by Fleck *et al.* (1995). Next, we examine the initiation of microbuckling from an elliptical region of initial fibre misalignment.

5.1. *Microbuckling from an infinite band of fibre waviness*

Consider a unidirectional composite plate subjected to remote compressive stress σ^∞ parallel to the fibre direction. It is assumed that the plate contains a band of fibre waviness, of infinite length and finite width w, as shown in Fig. 5. We align the x_1 co-ordinate with the remote fibre direction, and the x_2 co-ordinate with the transverse direction. The normal $\mathbf{n}$ to the band is rotated an angle β about the x_3-axis; then, the initial fibre misalignment is perfectly correlated along the direction $dx_2/dx_1 = -\tan\beta$. Fleck *et al.* (1995) have used a simplified form of couple stress theory to determine the effect on the compressive strength of the magnitude and wavelength of fibre misalignment within the infinite band. They restricted attention to the early stages of microbuckling where fibre rotations and strains remain small. This problem is revisited using our finite element code which can deal with finite deformation, and the effects of fibre extensibility and longitudinal shear.

Compressive failure is perceived to occur by the initiation and growth of a microbuckle from a finite imperfection in the form of fibre waviness, a void or a resin-rich region. It is reasonable to assume that an infinite band analysis is representative of the collapse response when the initial imperfection spans many fibre diameters in the transverse direction. In the current paper we shall explore the validity of the infinite band assumption.

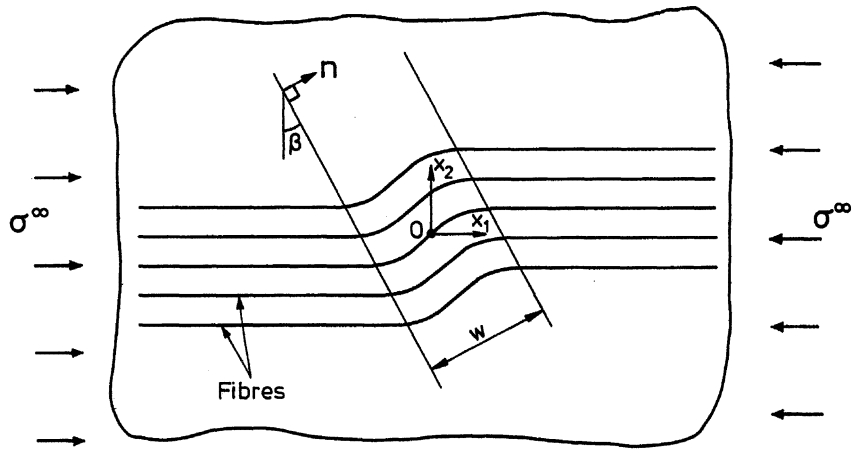

Fig. 5. Geometry of an infinitely long microbuckle band.

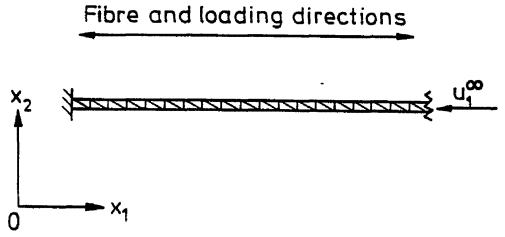

Fig. 6. The mesh for analysing the infinitely long microbuckle band of $\beta = 0°$; the mesh has 120 elements and 363 nodes.

Following Fleck *et al.* (1995) we adopt a cosine variation of initial fibre misalignment $\bar{\phi}$ with co-ordinate x_1' measured along the normal **n** to the band,

$$\bar{\phi} = \phi_0 \cos\frac{\pi x_1'}{w}, \quad x_1' = x_1 \cos\beta + x_2 \sin\beta. \tag{5.1}$$

Throughout the current paper we assume, arbitrarily, that the initial band width is $w = 20d$, where d is the fibre diameter. [Fleck *et al.* (1995) show that the compressive strength is relatively insensitive to the chosen value for w/d.] A typical finite element mesh is shown in Fig. 6. The mesh is aligned with the remote fibre direction and consists of six-node triangular elements (see Appendix B); it is of length $200d$ and of width $0.5d$. We exploit the rotational symmetry of the geometry and loading by extending the mesh over only half of the plane: the mesh is drawn from the centre of the band to a remote boundary. Vanishing displacement is prescribed at the left-hand end of the mesh and a uniform displacement u_1^∞ is applied at the right-hand end of the mesh. The torque traction vanishes at both ends. Periodic boundary conditions are applied to the sides of the mesh in order to reproduce the infinite band response. The calculation gives the remote stress σ^∞ which varies by less than 0.1% across the height of the mesh. A typical curve of the average value of σ^∞ versus the end displacement u_1^∞ is shown in Fig. 7(a), for the case $\bar{\phi}_0/\gamma_y = 4$ ($\bar{\phi}_0 = 2.3°$), $\beta = 0°$ and

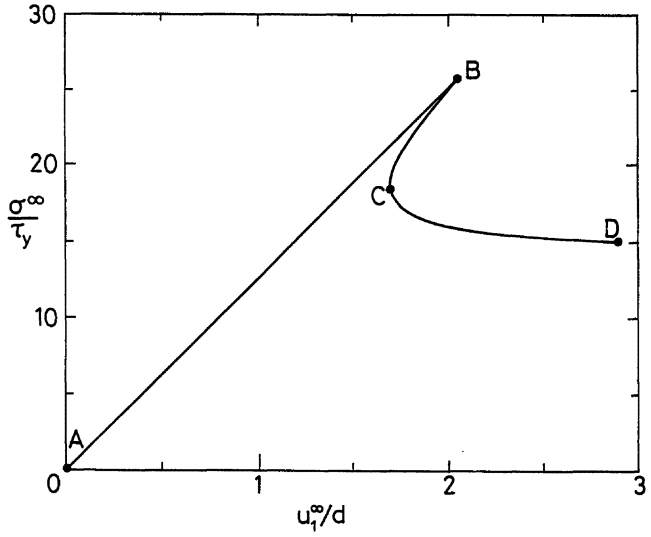

Fig. 7(a). A typical load versus end shortening displacement curve showing a snap-back response. $\bar{\phi}_0/\gamma_y = 4$, $\beta = 0°$ and $n = 3$.

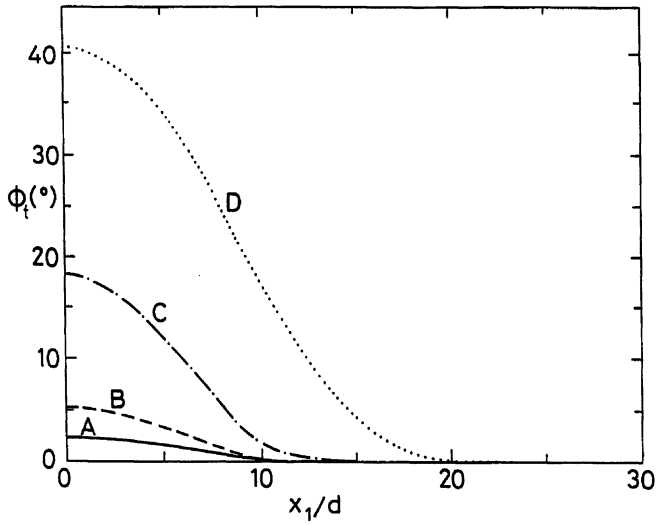

Fig. 7(b) The profile of fibre rotation angle along the fibre direction during the course of the loading history for an infinite microbuckle band. The labels A, B, C and D refer to the four stages of deformation given in Fig. 7(a).

$n = 3$.† The calculated compressive strength σ_c is within 1% of the values given in Fleck *et al.* (1993). Figure 7(a) displays a snap-back behaviour whereby the post-maximum load state is unstable under either a fixed remote load or a fixed remote displacement; the extent of the snap-back depends upon the length of the plate, as discussed by Kyriakides *et al.* (1995). The profile of total fibre rotation ϕ_t is plotted in Fig. 7(b) as a function of the x_1 co-ordinate (parallel to the remote fibre direction), at the four stages of loading history marked on Fig. 7(a). We note from Fig. 7(b) that the maximum load (labelled B) is associated with a small fibre rotation $\phi \approx 3°$ at the centre of the microbuckle band ($x_1 = 0$). At loads beyond the maximum load fibres within the band continue to rotate and the band of rotated fibres broadens.

The compressive strength is found to be relatively insensitive to the axial and shear moduli of the composite by the following parametric study. When the ratio E_L/τ_y is increased from 10^3 to 5×10^3, corresponding to an increase in E_L/E_T ratio from 4 to 20, the compressive strength increases by about 10%. Similarly, the compressive strength increases by less than 2% when G_f/τ_y is increased from 200 to 800. (Other moduli are held fixed at the values specified at the end of Section 4 and $n = 3$.)

5.2. *Microbuckling from an elliptical region of fibre waviness*

Next, we study the effect of a finite region of initial fibre misalignment upon the collapse response of the composite. Again, a uniform remote compressive stress σ^∞ is applied in the x_1-direction, as shown in Fig. 8(a). Consider the case where the initial fibre misalignment is confined to an ellipse of length l and width w in the (x_1, x_2) plane, as shown in Fig. 8(a). The axes of the ellipse (x_1', x_2') are rotated through an

† These values were chosen to be representative for carbon fibre–epoxy matrix composites as discussed by Budiansky and Fleck (1993); the compressive strength is a minimum for $\beta = 0°$ and is only mildly sensitive to the magnitude of β (see Fleck *et al.*, 1995).

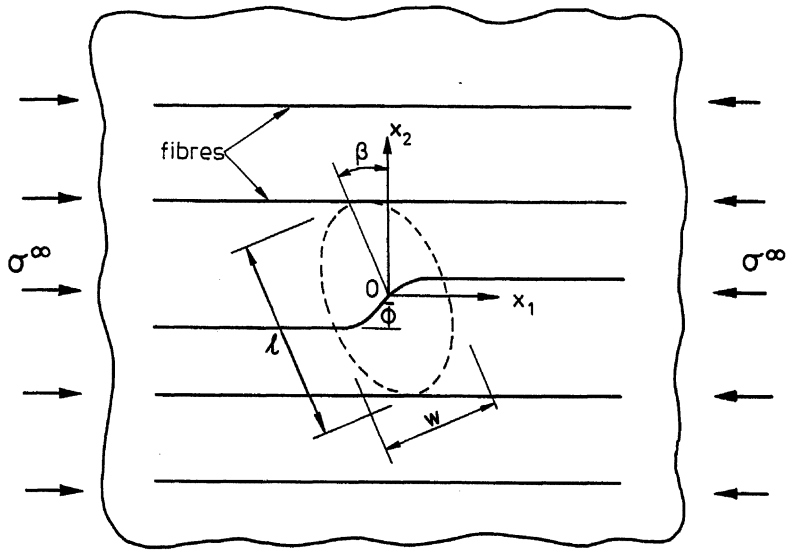

Fig. 8(a). Sketch of the initial imperfection. Fibre misalignment $\bar{\phi}$ is confined to an ellipse of length l and width w.

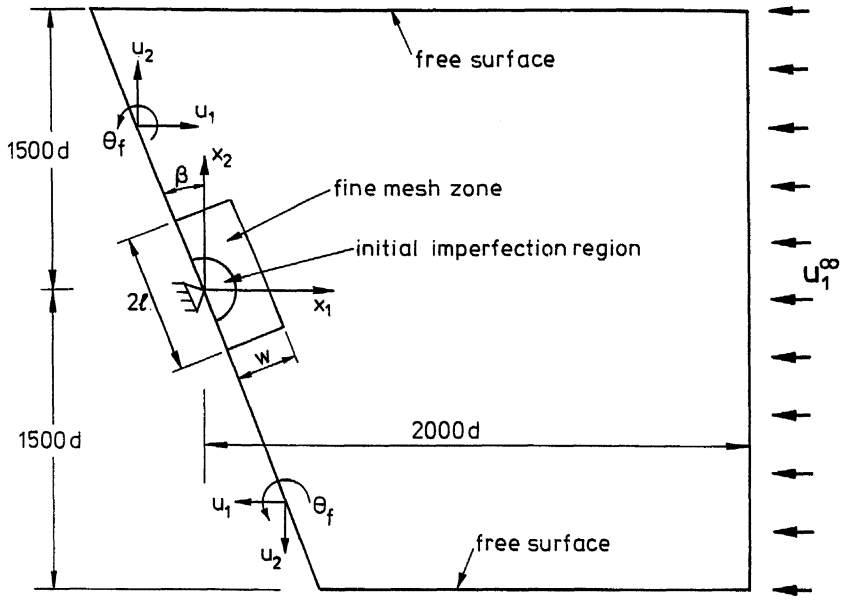

Fig. 8(b) Sketch of the geometry and boundary conditions for the case of a finite imperfection.

angle β about the x_3-axis with respect to (x_1, x_2) axes, such that

$$x_1' = x_1 \cos\beta + x_2 \sin\beta \quad \text{and} \quad x_2' = -x_1 \sin\beta + x_2 \cos\beta. \tag{5.2}$$

In the region exterior to the ellipse the fibres are straight and perfectly aligned in the x_1-direction. The fibre misalignment follows a cosine distribution within the elliptical region, as specified by

$$\bar{\phi} = \begin{cases} \bar{\phi}_0 \cos\dfrac{\pi}{2}\rho, & \text{if } \rho < 1; \\ 0, & \text{if } \rho \geqslant 1. \end{cases} \tag{5.3}$$

where

$$\rho \equiv \left\{ \left(\frac{2x_1'}{w} \right)^2 + \left(\frac{2x_2'}{l} \right)^2 \right\}^{1/2}. \tag{5.4}$$

As the band length $l \to \infty$, the imperfection tends to an infinite band as described in the previous section. At the other limit of $l \to 0$, the fibre misalignment vanishes and the compressive strength σ_c approaches the Rosen value of $\sigma_c = G$, where G is the in-plane shear modulus of the composite. These limits provide a useful check to our finite element calculations.

A sketch of the geometry and the boundary conditions is shown in Fig. 8(b); we need to consider only half of the structure due to the rotational symmetry of the imperfection and of the remote loading. The plate is loaded by a uniform remote displacement u_1^∞ and the finite element calculation gives the corresponding remote stress σ^∞. (For all the cases reported below σ^∞ varies by less than 0.1% over the end of the structure.) A typical undeformed mesh is given in Fig. 9(a) and the region of fine mesh containing the imperfection is shown in Fig. 9(b). The dashed line indicates the boundary of the initial imperfection region. The full mesh is of length $2000d$ and of width $3000d$.

A typical plot of the average remote stress σ^∞ versus the end shortening u_1^∞ is given in Fig. 10 for the inclinations $\beta = 0°$ and $\beta = 30°$ ($n = 3$, $\bar{\phi}_0/\gamma_y = 4$, $w/d = 20$, $l/d = 50$). The two responses are almost linear with a sharp snap-back behaviour at maximum load. In order to distinguish between the two responses, the response for $\beta = 30°$ has been shifted horizontally in Fig. 10. Since we focus our attention on the

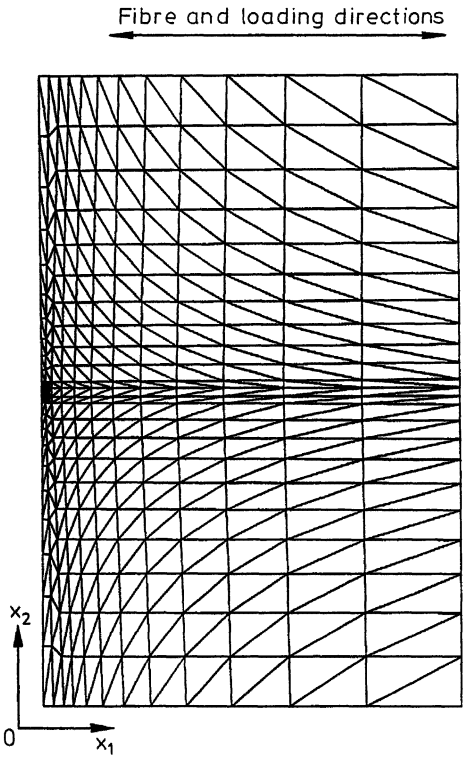

Fig. 9(a). Global view of a typical undeformed mesh with 1985 elements and 4066 nodes.

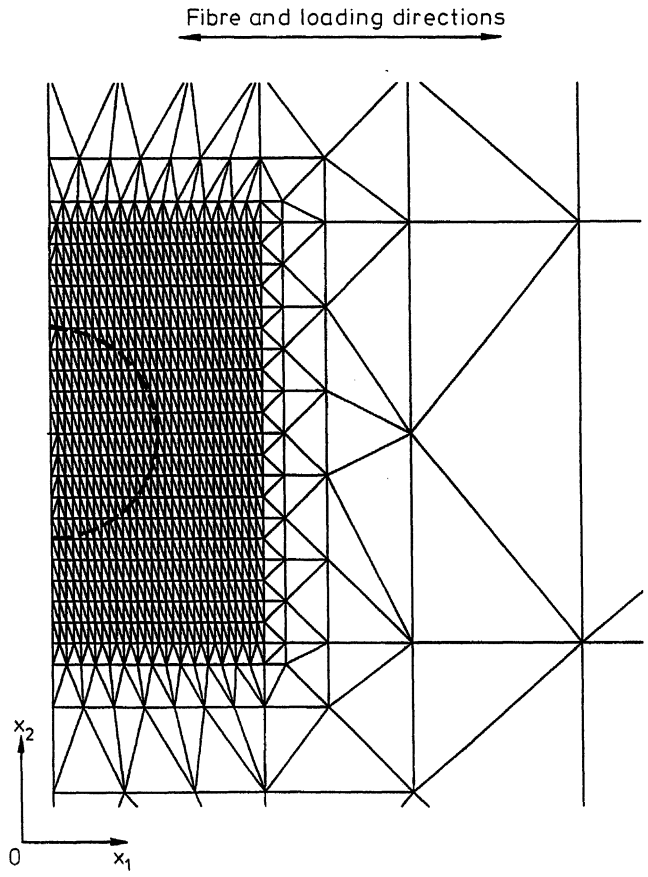

Fig. 9(b). The fine mesh zone of the mesh shown in Fig. 9(a). The dashed line indicates the boundary of the initial imperfection region.

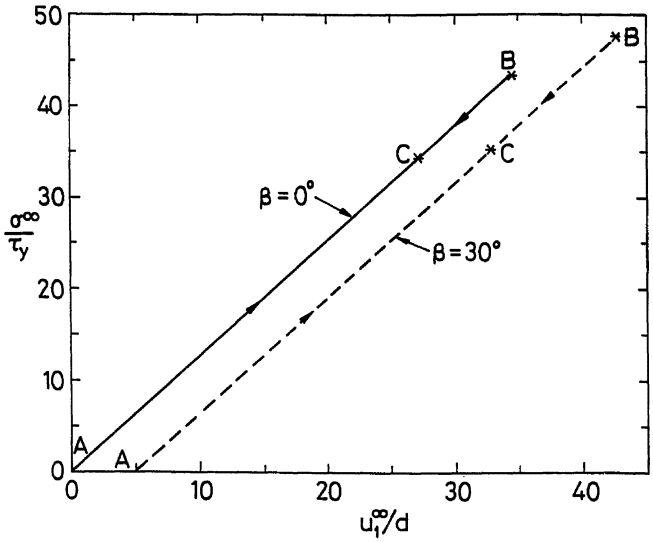

Fig. 10. Remote stress σ^∞ versus end displacement u_1^∞ response for a finite imperfection of $l/d = 50$, $n = 3$ and $\bar{\phi}_0/\gamma_y = 4$. The responses shown for $\beta = 0°$ and $\beta = 30°$ are almost indistinguishable except for different maximum loads. ($\sigma_c/G = 0.435$ for $\beta = 0°$ and $\sigma_c/G = 0.478$ for $\beta = 30°$.)

initiation and early propagation of a microbuckle, the calculation of the post-buckling response was stopped when the load dropped to about 75% of the maximum load. The severe snap-back responses of Fig. 10 are due to the fact that the mesh is long in the fibre direction ($2000d$). The snap-back is more severe than in the infinite band case of Fig. 7(a) as the fibres surrounding the finite imperfection remain almost straight at maximum load.

The progressive nature of the collapse is exhibited by contours of total fibre rotation ϕ_t, which are shown in Fig. 11 for $\beta = 0°$ and in Fig. 12 for $\beta = 30°$. For both geometries contours are displayed for states A, B and C as labelled on Fig. 10. State A is the initial unloaded configuration with $\phi = 0$ and $\phi_t = \bar{\phi}$; state B is immediately post maximum load (99.7% of maximum load for $\beta = 0°$ and 99.6% of maximum load for $\beta = 30°$); and state C is at 78% of maximum load for $\beta = 0°$ and 74% maximum load for $\beta = 30°$. We note that state B, at just past maximum load, displays:

(i) a relatively small maximum value of fibre rotation $\phi = \phi_t - \bar{\phi}$. The maximum fibre rotation is $\phi = 4.4°$ for the case $\beta = 0°$, and the maximum fibre rotation is $\phi = 3.9°$ for the case $\beta = 30°$;
(ii) a spatially small region of fibre rotation. For example, consider the case $\beta = 0°$. At maximum load the region over which the total fibre rotation exceeds 0.5° is only $70d$, i.e. 2.3% of the width of the mesh.

We note from Figs 11 and 12 that, regardless of the initial orientation β of the region of waviness, the microbuckle band tends to propagate in the transverse x_2-direction. Considerable compressive transverse strain of about 4% is attained at state C. This suggests that the phenomenon of "fibre lock-up" may need to be considered, as described by Fleck and Budiansky (1991). However, further work is required in order to determine whether "fibre lock-up" has a significant effect on determining the propagation angle β of a microbuckle band.†

The effect upon the collapse strength σ_c of the initial length l and orientation β of the imperfection is shown in Figs 13(a) and (b) respectively. Consider first Fig. 13(a). As the length l increases from zero to infinity, the collapse strength decreases from the elastic bifurcation strength $\sigma_c = G$ given by Rosen (1965) to the infinite band result given by Fleck *et al.* (1995). The collapse strength is mid-way between the elastic bifurcation value and the infinite band value at a "transition length" $l/d \approx 20$. For $l > 0$, the strength decreases with increasing magnitude of initial misalignment $\bar{\phi}_0$ and with increasing strain hardening index n.

An analytical formula for compressive strength has been given by Budiansky and Fleck (1993) for an infinite band, inclined at an inclination β as

$$\frac{\sigma_c}{G} = \frac{1 + R^2 \tan^2 \beta}{1 + n\left(\frac{3}{7}\right)^{\frac{1}{n}} \left[\frac{\bar{\phi}_0/\gamma_Y}{n-1} \sqrt{1 + R^2 \tan^2 \beta}\right]^{\frac{n-1}{n}}}. \tag{5.5}$$

† The authors have recently included the effects of lock-up in the finite element analysis. Initial results for a finite circular initial imperfection suggest that the microbuckle initiates at a vanishing angle β and then grows with an increasing value of β. In the early stages of growth the microbuckle is inclined at about $\beta = 10°$, in agreement with the findings of Kyriakides *et al.* (1995).

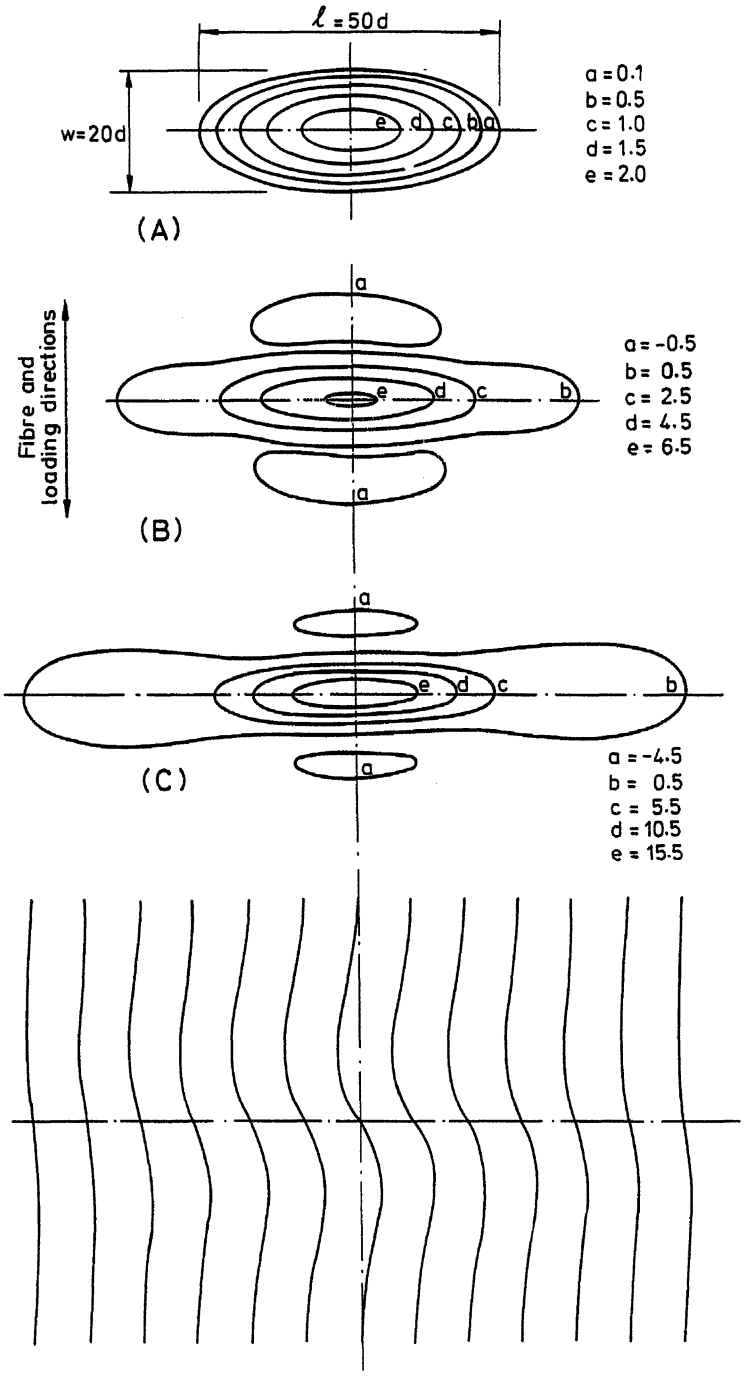

Fig. 11. Contours of total fibre rotation ϕ_t (in degrees) at the three stages marked A, B and C in Fig. 10 for $\beta = 0°$. Remote stresses at stages B and C are respectively 99.7 and 78.2% of the maximum load. The shape of the deformed fibres at state C is included at the bottom of the figure.

The parameters in (5.5) have already been defined above. Although this formula was derived using the so-called *kinking* analysis (neglecting fibre bending) it has been shown by Fleck *et al.* (1995) that the strengthening associated with fibre bending is negligible for $w/d \leqslant 20$. For a typical initial band width of $w = 20d$, it is seen from Fig. 13(a) that σ_c exceeds the infinite band strength by less than 20% for a length of

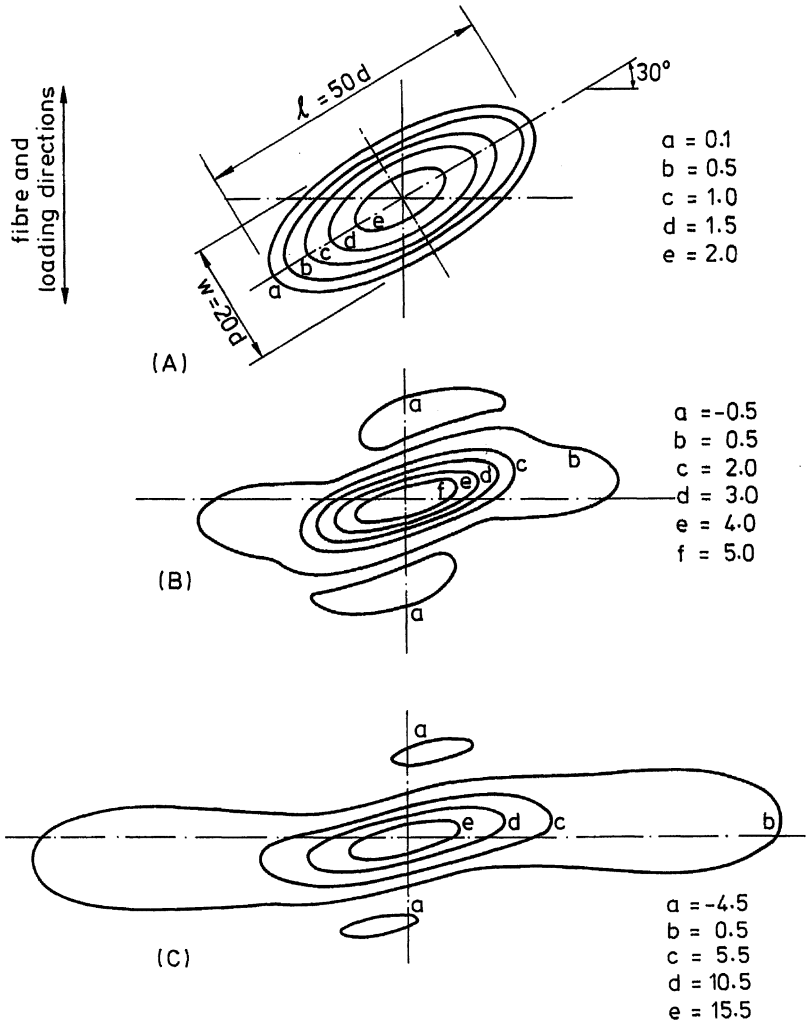

Fig. 12. Contours of the total fibre rotation ϕ_t (in degrees) at the three stages marked as A, B and C in Fig. 10 for $\beta = 30°$. Remote stresses at B and C are respectively 99.6 and 73.8% of the maximum load.

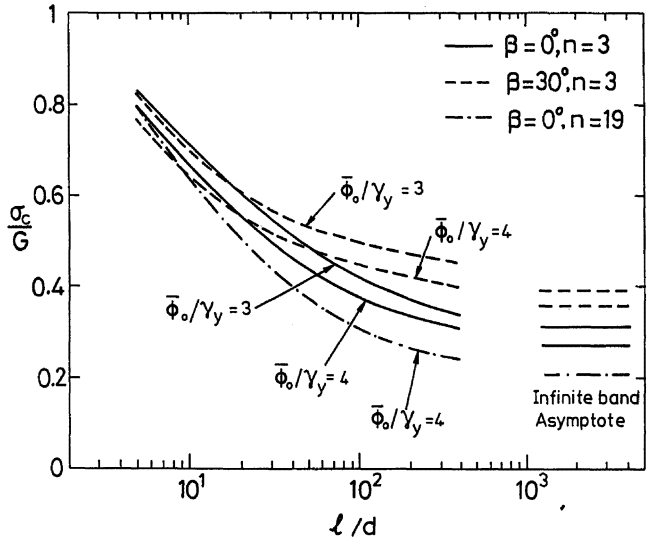

Fig. 13(a). Compressive strength as a function of the length l of the elliptical region of fibre misalignment. $w/d = 20$. The infinite band results are taken from Fleck *et al.* (1995).

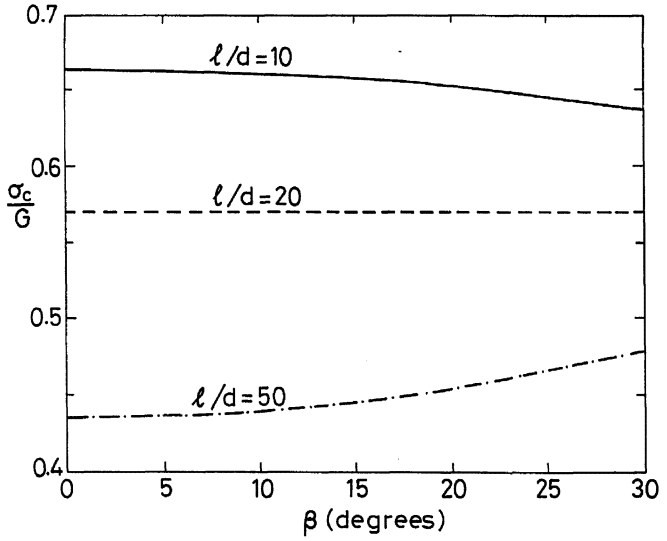

Fig. 13(b). The effect of the orientation β of the elliptical region of waviness on the compressive strength. $n = 3$, $w/d = 20$ and $\bar{\phi}_0/\gamma_y = 4$.

waviness l greater than $400d$. For typical carbon fibre–epoxy composites, the fibre diameter is approximately 5 μm : we conclude that the estimate (5.5) from the infinite band kinking model is adequate provided the region of initial waviness exceeds about 2 mm in length.

The effect of the initial band inclination β upon σ_c depends upon the value of l/d, as shown in Fig. 13(b). Recall that the width w of the elliptical region of waviness has been set at $w/d = 20$ throughout. Thus, the imperfection is circular at $l/d = 20$. At $l/d > 20$ the ellipse is elongated in the direction which subtends an angle β with the x_2-axis, and σ_c increases with increasing β. At $l/d < 20$ the ellipse is elongated in the direction which subtends an angle β with the x_1-axis, and σ_c decreases with increasing β.

Ohno and Hutchinson (1984) have performed an analogous exploratory study of the effect of a finite imperfection on localisation in metals. They considered localisation in a circular bar under axisymmetric loading. The initial imperfection was a central region of reduced strength due to an enhanced void content compared to the remainder of the voided solid. Their results are qualitatively similar to those presented here : as the aspect ratio l/w of the imperfection increases the ductility goes through a transition from a high value (corresponding to bifurcation of the solution for a uniformly voided solid) to a lower value (corresponding to an infinite band solution with enhanced voiding within the band).

6. CONCLUSIONS

A finite element code based on general Cosserat couple stress theory has been developed for analysing the plastic microbuckling of a fibre composite from an initial imperfection in the form of a localised region of fibre waviness. A unit cell analysis gives the same governing equations as those of Cosserat couple stress theory and

clarifies the physical meaning of the independent micro-rotation. As the length of the imperfection is increased from zero to infinite, the compressive strength drops from the Rosen (1965) value of the in-plane shear modulus of the composite to the infinite band strength of Fleck *et al.* (1995). The results show that the compressive strength is mid-way between the two limits for a circular imperfection of diameter $20d$, where d is the fibre diameter. The infinite band approximation is accurate to within 20% when the imperfection length exceeds about $400d$, i.e. about 2 mm for carbon fibre–epoxy composites.

ACKNOWLEDGEMENTS

The authors wish to thank Prof. B. Budiansky and Dr M. P. F. Sutcliffe for many helpful discussions. Financial support from the ONR grant 0014-91-J-1916 is gratefully acknowledged. Additional financial support is acknowledged from the Defence Research Agency, Farnborough.

REFERENCES

Argon, A. S. (1972) Fracture of composites. *Treatise of Materials Sciences and Technology*, Vol. 1. Academic Press, New York.

Budiansky, B. (1983) Micromechanics. *Comp. Struct.* **16**(1), 3–12.

Budiansky, B. and Fleck, N. A. (1993) Compressive failure of fibre composites. *J. Mech. Phys. Solids* **41**, 183–211.

Budiansky, B. and Fleck, N. A. (1994) Compressive kinking of fibre composites: a topical review. *Appl. Mech. Rev.* **47**(6), part 2, S246–S270, June.

Cosserat, E. and Cosserat, F. (1909) *Theorie des Corps Deformables*. Herman et fils, Paris.

Crisfield, M. A. (1991) *Non-linear Finite Element Analysis of Solids and Structures*, Vol. 1, Chapter 9. John Wiley & Sons, U.K.

Fleck, N. A. and Budiansky, B. (1991) Compressive failure of fibre composites due to micro-buckling. *Inelastic Deformation of Composite Materials* (ed. G. J. Dvorak), pp. 235–274. Springer-Verlag.

Fleck, N. A., Deng, L. and Budiansky, B. (1995) Prediction of kink widths in compressed fiber composites. *J. Appl. Mech.* **62**, 329–337.

Hutchinson, J. W. and Tvergaard, V. (1981) Shear band formation in plane strain. *Int. J. Solids Struct.* **17**, 451–470.

Koiter, W. T. (1964) Couple stresses in the theory of elasticity, I and II. *Proc. Ned. Akad. Wet.* (*B*) **67**(1), 17–44.

Kyriakides, S., Arseculeratne, R., Perry, E. J. and Liechti, K. M. (1995) On the compressive failure of fibre reinforced composites. *Int. J. Solids Struct.* **32**(6/7), 689–738.

Mindlin, R. D. (1964) Micro-structure in linear elasticity. *Arch. Rat. Mech. Anal.* **16**, 51–78.

Mindlin, R. D. and Tiersten, H. F. (1962) Effects of couple-stress in linear elasticity. *Arch. Rat. Mech. Anal.* **11**, 415–448.

Ohno, N. and Hutchinson, J. W. (1984) Plastic flow localization due to non-uniform void distribution. *J. Mech. Phys. Solids* **32**(1), 63–85.

Rice, J. R. (1976) The localization of plastic deformation. *Theoretical and Applied Mechanics* (ed. W. T. Koiter), pp. 207–220. North-Holland Publishing Co., Amsterdam.

Rosen, B. W. (1965) Mechanics of composite strengthening. *Fibre Composite Materials*, pp. 37–75. Am. Soc. Metals Seminar, Metals Park, Ohio.

Slaughter, W. S., Fleck, N. A. and Budiansky, B. (1993) Microbuckling of fibre composites: the roles of multi-axial loading and creep. *J. Engng Mater. Technol.* **115**(3), 308–313.

Toupin, R. A. (1962) Perfectly elastic materials with couple-stresses. *Arch. Rat. Mech. Anal.* **11,** 385–414.

Zienkiewicz, O. C. and Taylor, R. L. (1989) *Finite Element Method,* Vol. 1, 4th Ed. McGraw-Hill, U. K.

APPENDIX A: REVIEW OF COSSERAT COUPLE STRESS THEORY

The classical theories of continuum mechanics (such as elasticity and plasticity theories) assume that the transmission of loads on both sides of an infinitesimal surface element $\mathrm{d}S$ within the material is described completely by a force vector $\mathbf{T}\,\mathrm{d}S$ acting on the surface element. In the couple stress theory of Cosserat and Cosserat (1909) it is assumed that the surface element $\mathrm{d}S$ may transmit both a force vector $\mathbf{T}\,\mathrm{d}S$ and a couple vector $\mathbf{Q}\,\mathrm{d}S$. The corollary is that the deformation field of the body is specified by a material rotation $\boldsymbol{\theta}$ in addition to the displacement field $\mathbf{u}$. Toupin (1962), Mindlin and Tiersten (1962) and Koiter (1964) have considered the so-called *reduced* couple stress theory, wherein $\boldsymbol{\theta}$ is identified with the rotation of the displacement field, $\boldsymbol{\theta} \equiv \frac{1}{2}\mathrm{curl}\mathbf{u}$. Here we shall adopt the framework of general couple stress theory, as laid down by the Cosserat brothers (Cosserat and Cosserat, 1909).

Consider an arbitrary volume Ω of the body in the deformed configuration, bounded by a piecewise smooth surface S. Equilibrium of forces on the body gives

$$\int_S \mathbf{T}\,\mathrm{d}S = \mathbf{0} \tag{A.1}$$

and equilibrium of moments gives

$$\int_S [\mathbf{X}\times\mathbf{T}+\mathbf{Q}]\,\mathrm{d}S = \mathbf{0} \tag{A.2}$$

where $\mathbf{X}$ is the radius vector from an arbitrary fixed point, and body forces and body couples have been neglected. Now introduce the Cartesian base vectors $\mathbf{e}_i$. The components σ_{ij} of the unsymmetric Cauchy stress tensor $\boldsymbol{\sigma}$ denote the components of T_j on a plane with a unit normal n_i such that

$$T_j = n_i\sigma_{ij}. \tag{A.3}$$

(Throughout this Appendix a repeated suffix denotes summation over 1 to 3.) In similar manner, the components m_{ij} of the couple stress tensor $\mathbf{m}$ denote the components of Q_j on a plane with a unit normal n_i, giving

$$Q_j = n_i m_{ij}. \tag{A.4}$$

Application of the divergence theorem to (A.1) and (A.2), using (A.3) and (A.4), leads to the usual force equilibrium equation

$$\sigma_{ji,j} = 0 \tag{A.5}$$

and the moment equilibrium equation

$$\varepsilon_{ijk}\sigma_{jk} + m_{ji,j} = 0 \tag{A.6}$$

where the comma subscript denotes differentiation with respect to a component of the spatial co-ordinate $\mathbf{X}$. The three-dimensional permutation symbol is designated ε_{ijk}.

The principle of virtual work is formulated in terms of virtual displacements δU_i and *independent* virtual rotations $\delta\Theta_i$; only for the special case of reduced Cosserat theory does $\delta\Theta_i$

coincide with the material rotation. Denote the rate at which work is absorbed internally per unit volume by δw; then, the equation of virtual work reads

$$\int_\Omega \delta w \, d\Omega = \int_S [T_i \delta U_i + Q_i \delta \Theta_i] \, dS \tag{A.7}$$

where the volume Ω is contained within the closed surface S. Using the divergence theorem, the right-hand side of (A.7) may be re-arranged to the form

$$\int_S [T_i \delta U_i + Q_i \delta \Theta_i] \, dS = \int_\Omega [\sigma_{ji,j} \delta U_i + (\varepsilon_{ijk} \sigma_{jk} + m_{ji,j}) \delta \Theta_i + \sigma_{ij} \delta \gamma_{ji} + m_{ij} \delta \kappa_{ji}] \, d\Omega \tag{A.8}$$

where the increment in "relative strain" is $\delta \gamma_{ij} \equiv \delta U_{i,j} + \varepsilon_{ijk} \delta \Theta_k$, and the curvature increment is $\delta \kappa_{ij} \equiv \delta \Theta_{i,j}$. Consider the right-hand side of (A.8). The first term vanishes by force equilibrium (A.5), and the second term vanishes by moment equilibrium (A.6). Thus, the principle of virtual work follows from (A.8) as

$$\int_S [T_i \delta U_i + Q_i \delta \Theta_i] \, dS = \int_\Omega [\sigma_{ij} \delta \gamma_{ji} + m_{ij} \delta \kappa_{ji}] \, d\Omega. \tag{A.9}$$

APPENDIX B: FINITE ELEMENT IMPLEMENTATION

A Lagrangian formulation is adopted to deal with the finite deformation of the composite. The mesh is drawn in the initial undeformed configuration and, at each loading step, the Cartesian components of the displacement increments are calculated; summation gives the accumulated displacement. A 6-noded triangular element is adopted, with three degrees of freedom at each node: (u_1, u_2, θ_f) as shown in Fig. B1. The displacement and velocity fields are interpolated as

$$u_1 = \sum_{I=1}^{6} N^I u_1^I, \quad u_2 = \sum_{I=1}^{6} N^I u_2^I, \quad \theta_f = \sum_{I=1}^{6} N^I \theta_f^I, \tag{B.1}$$

$$v_1 = \sum_{I=1}^{6} N^I v_1^I, \quad v_2 = \sum_{I=1}^{6} N^I v_2^I, \quad \dot{\theta}_f = \sum_{I=1}^{6} N^I \theta_f^I \tag{B.2}$$

where the superscript I indicates the respective values at node I. The shape functions are defined by

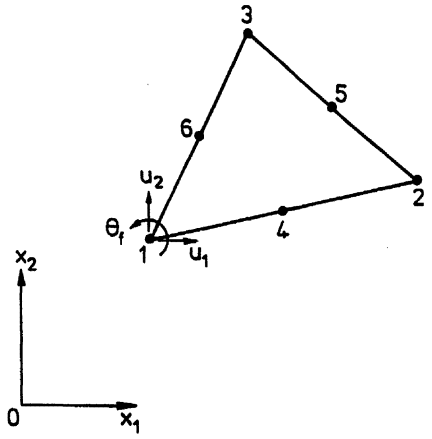

Fig. B1. The six-noded triangular element and its degrees of freedom.

$$N^I = \lambda^I(2\lambda^I - 1) \quad \text{for} \quad I = 1,2,3 \tag{B.3}$$

and

$$N^4 = 4\lambda^1\lambda^2, \quad N^5 = 4\lambda^2\lambda^3, \quad N^6 = 4\lambda^3\lambda^1. \tag{B.4}$$

The definition of the triangular area co-ordinates λ^I can be found in standard finite element text books such as Zienkiewicz and Taylor (1989).

The physical components of the velocity and displacement in terms of the orthonormal base vector $(\boldsymbol{\varepsilon}_1, \boldsymbol{\varepsilon}_2)$ in the deformed configuration follow from (B.1) and (B.2) as

$$U_1 = \sum_{I=1}^{6} N^I(u_1^I \cos\phi_t + u_2^I \sin\phi_t), \quad U_2 = \sum_{I=1}^{6} N^I(-u_1^I \sin\phi_t + u_2^I \cos\phi_t) \tag{B.5}$$

and

$$V_1 = \sum_{I=1}^{6} N^I(v_1^I \cos\phi_t + v_2^I \sin\phi_t), \quad V_2 = \sum_{I=1}^{6} N^I(-v_1^I \sin\phi_t + v_2^I \cos\phi_t) \tag{B.6}$$

where

$$\cos\phi_t = \frac{F_{11}\cos\bar{\phi} + F_{12}\sin\bar{\phi}}{\Lambda}, \quad \sin\phi_t = \frac{F_{21}\cos\bar{\phi} + F_{22}\sin\bar{\phi}}{\Lambda}. \tag{B.7}$$

Here, $\bar{\phi}$ is the initial fibre misalignment angle, and the Cartesian components of the deformation gradient tensor $\mathbf{F}$ are defined by

$$F_{ij} = \frac{\partial X_i}{\partial x_j} = \delta_{ij} + \frac{\partial u_i}{\partial x_j}. \tag{B.8}$$

The denominator Λ of (B.7) is

$$\Lambda = \{(F_{11}\cos\bar{\phi} + F_{12}\sin\bar{\phi})^2 + (F_{21}\cos\bar{\phi} + F_{22}\sin\bar{\phi})^2\}^{1/2}. \tag{B.9}$$

The finite element formulation is used to set up a linear system of equations with the nodal velocities as the primary unknowns. The tangent stiffness matrix of the system of equations is determined from the rate form of the principle of virtual work, (3.27) as follows. The stress rate $\dot{\sigma}_{ij}$ is expressed in terms of the velocity gradient D_{ij} and the couple stress rate $\dot{m}_1$ is expressed in terms of the curvature rate $\dot{\kappa}_1$ via the constitutive equations (4.1)–(4.3) and (4.15). To carry out the volume integration of the virtual work statement over each element, a seven-point Gauss–Radau quadrature rule (Zienkiewicz and Taylor, 1989) is adopted. Since θ_f has quadratic variation in x_i, the term $(\dot{\sigma}_{21} - \dot{\sigma}_{12})\delta\dot{\theta}_f$ contains a term $\dot{\theta}_f\delta\dot{\theta}_f$ which is a fourth order polynomial of x_i. To integrate such a term exactly, the seven-point Gauss–Radau quadrature is used. (A selected reduced integration is not needed since the fibre shear stiffness is small.) The above procedure gives us a system of linear equations for the unknown nodal velocity $\mathbf{v}$ and rotation $\dot{\theta}_f$.

In order to calculate the stiffness matrix of the overall system of equations in rate form, the following equations relating differentiation in the curvilinear co-ordinates (in the deformed configuration) to differentiation in Cartesian co-ordinates (in the undeformed configuration) are required:

$$\left.\begin{aligned} \frac{\partial}{\partial s_1} &= (F_{12}^{-1}\cos\phi_t - F_{11}^{-1}\sin\phi_t)\frac{\partial}{\partial x_1} + (F_{22}^{-1}\cos\phi_t - F_{21}^{-1}\sin\phi_t)\frac{\partial}{\partial x_2} \\ \frac{\partial}{\partial s_2} &= (F_{11}^{-1}\cos\phi_t + F_{12}^{-1}\sin\phi_t)\frac{\partial}{\partial x_1} + (F_{21}^{-1}\cos\phi_t + F_{22}^{-1}\sin\phi_t)\frac{\partial}{\partial x_2} \end{aligned}\right\} \tag{B.10}$$

where F_{ij}^{-1} is the ijth Cartesian component of the inverse of $\mathbf{F}$. Since the Cartesian co-ordinate

in the undeformed configuration x_i is a linear function of the area co-ordinates λ_i and vice versa, the conversion between $\partial/\partial x_i$ and $\partial/\partial\lambda_i$ is straightforward, and is not presented here.

The components of the virtual displacement and velocity gradients in the curvilinear co-ordinates are calculated via

$$W_{ij} = \boldsymbol{\varepsilon}_j \cdot \frac{\partial \delta \mathbf{u}}{\partial s_i} \quad \text{and} \quad D_{ij} = \boldsymbol{\varepsilon}_j \cdot \frac{\partial \mathbf{v}}{\partial s_i} \tag{B.11}$$

and the virtual curvature $\delta\kappa_1$ and curvature rate $\dot{\kappa}_1$ are calculated via

$$\delta\kappa_1 = \frac{\partial \delta\theta_f}{\partial s_1} \quad \text{and} \quad \dot{\kappa}_1 = \frac{\partial \dot{\theta}_f}{\partial s_1}. \tag{B.12}$$

To deal with the snap-back effect, we employ a version of the modified Riks algorithm by Crisfield (1991). The linearised arc-length method is chosen because of its simplicity, and the sign of the determinant of the current tangent stiffness matrix determines the loading direction of the next increment. The convergence criterion for the equilibrium iterations is such that the absolute value of any residual nodal force (the applied nodal forces subtracted by the nodal forces in balancing with the internal stresses and couple stress) is less than a given tolerance (which is set to be $10^{-3}\,\tau_y d$ for force and $10^{-3}\,\tau_y d^2$ for torque).